UNIVERSITY COLLEGE LONDON

Department of Physics & Astronomy

Sterile neutrino decays with an exotic axion-like extension

MSc Research Thesis

Author: Jan Wawrzynek

Supervisors: Professors Frank Deppisch and Robert Thorne

Degree course: MSc Physics

August, 2025

Abstract

Heavy Neutral Leptons (HNLs) are an exotic species of Majorana neutrinos, which has noted significant attention in recent years due to the particles ability to resolve 3 important Beyond Standard Model (BSM) phenomena: neutrino oscillations, baryon asymmetry and dark matter. This thesis develops a python simulation engine, to explore the decay and abundance properties of such HNLs, whose dominant decays are into Axion-like particles (ALPs). To achieve this an object-oriented programming approach was undertaken to develop a modular and easily extendable python engine, which is capable of easily incorporating additional exotic particle and decays for future study. The branching ratios for HNLs were calculated for a range of HNL masses, mixing angles and ALP properties. Iso-lifetime contours were obtained in the $(m_{N_i}, |U_{\ell N}|^2)$ plane for the three sterile neutrino flavours, showcasing potentially promising avenues of experimental search. Thermally averaged decay rates for the HNLs and ALPs were calculated to provide a framework for extending the code into cosmological applications.

Contents

1 Introduction

Heavy Neutral Leptons (HNLs) are a popular extension of the Standard Model (SM) as they can explain a number of beyond SM phenomena, such as neutrino oscillations as HNLs allow for mechanisms producing neutrino masses, like the type 1: Seesaw Mechanism which we will explore in this study. These exotic particles are charge-neutral fermions which act as heavy right handed neutrinos. HNLs also provide a mechanism for generating the matter-antimatter asymmetry of the universe, as their CP-violating decays or oscillations could produce a baryon asymmetry through leptogenesis. [1–3]. Multiple experiments have been proposed with the explicit aim to search for HNLs: DUNE [4], NA62 [5–7], SHiP [8,9], CODEX-b [10], MATH-USLA [11–14], FASER [15–17]. Searches have already been performed at LHCb, CMS, ATLAS, T2K and Belle. However, the parameter space of these HNLs is heavily constrained due to factors like Big Bang Nucleosynthesis (BBN), which puts a lower limit on possible HNL masses [18]. Without a new exotic decay channel, HNLs in thermal equilibrium that have a lifetime $\tau > 1$ s, would have a dominant decay into hadronic channels [19]. Crucially the mesons generated in such decays would interact strongly with the protons and neutrons in the primordial universe's plasma. Thus, changing the $p \leftrightarrow n$ conversion ratio, which decides the abundances required for BBN, particularly affecting ^{4}He [18] abundances.
In 2024, Deppisch et al. [19] introduced a model, expanding the SM particle spectrum by adding an axion-like particle (ALP) and a SM gauge singlet (HNL). Introducing a dominant decay channel for HNLs (N) to an ALP (a) and an active neutrino (ν), $N \to a\nu$, causes the HNLs to decay faster and hence, avoid the BBN bound for lesser HNL masses, provided that the ALPs decays much later than BBN ($\tau_a > 10^4$ s).

The central focus of this thesis is to create a modular and extendable python simulation engine for HNL decays. This engine will be used to build on the work of [19,20] by introducing the ALP dominant decay to an HNL model with mixing among three sterile neutrino flavours (N_1, N_2, N_3) with the goal of determining the $(m_N, |U_{\ell N}|^2)$ parameter space opened up by this extension for HNLs with the required lifetime of under 1 seconds to avoid damage to BBN. This will be shown using HNL iso-lifetime in the $(m_N, |U_{\ell N}|^2)$ plane.

In Section 2, I will illustrate the core theory behind neutrinos and HNLs. Section 3, details the mechanisms of HNL decays through charged-current and neutral-current processes in leptonic and hadronic three-body channels. Additionally it will incorporate the ALP decay for HNLs as well as provide a brief background introduction to ALP theory [19], albeit ALPs are not the main focus of this thesis. Section 4 describes the application of these HNL and ALP decays in Cosmology, particularly looking into the evolution of particle number densities in the early universe. Section 5 describes the computational methodology for this study, detailing how the python engine was engineered with reusability and extension in mind. Section 6 (Results) showcases iso-lifetime contour curves for the HNLs in the $(m_N, |U_{\ell N}|^2)$ plane, branching ratios for a range of ALP parameter values, as well as the evolution of HNL and ALP number densities in the early universe. Section 7 concludes the thesis by discussing the simulation results in relation to the estabilished literature, suggesting the results potential utility in narrowing down the parameter space of interest in upcoming HNL experimental searches as well as providing an outlook on how this research could be continued.

2 Neutrinos and the Standard Model

Force	Strength	Boson	Spin	Mass/GeV
Quantum Chromodynamics	1	Gluon g	1	0
Quantum Electrodynamics	10^{-3}	Photon γ	1	0
Weak	10^{-8}	W boson $W^{\pm}$	1	80.4
		Z boson Z	1	91.2

Table 1: Quantum Field Theories and their corresponding bosons, table acquired from [21].

	Leptons			Quarks		
Generation	**Particle**	**Charge**	**Mass/GeV**	**Particle**	**Charge**	**Mass/GeV**
1st	Electron (e^-)	-1	0.0005	Down (d)	$-1/3$	0.003
	Neutrino (ν_e)	0	$< 10^{-9}$	Up (u)	$+2/3$	0.005
2nd	Muon (μ^-)	-1	0.106	Strange (s)	$-1/3$	0.1
	Neutrino (ν_μ)	0	$< 10^{-9}$	Charm (c)	$+2/3$	1.3
3rd	Tau (τ^-)	-1	1.78	Bottom (b)	$-1/3$	4.5
	Neutrino (ν_τ)	0	$< 10^{-9}$	Top (t)	$+2/3$	174

Table 2: Standard Model Fermions, table acquired from [21]

The ensuing discussion follows [21] and provides a brief introduction to the SM and exotic particles featured in our model and the quantum field theories associated with them. The SM of Particle Physics details the elementary particles of the universe and all of the interactions between them discovered to date, except for the gravitational force. However, as the strength of the gravitational force is negligible on the energy scales relevant to this discussion, it will be neglected in this model. The three forces relevant to this discussion are Quantum Chromodynamics (QCD), Quantum Electrodynamics (QED) and in particular the weak force. Which are all described by Quantum Field Theories (QFTs). In such theories, particle interactions are mediated by the exchange of spin-1 force-carrying virtual particles known as gauge bosons. The last boson to be experimentally observed in the standard model, is the Higgs boson, a spin -0 scalar particle with $m_H \approx 125$ GeV. The Higgs boson is special, as it is responsible for the Higgs mechanism, which generates the mass for all other particles. However, the impact of the Higgs boson is not significant for the energy scales and particles of interest, therefore it will be neglected for this study. The SM also contains the 12 fundamental spin$-\frac{1}{2}$ particles and 12 corresponding antiparticles called fermions (the antiparticle of a particle has identical mass, but opposite quantum numbers (charge, baryon number, lepton number). To simplify the number of particles in this study, we will make use of symmetry and instead of incorporating the antiparticle variants of every possible interaction channel, we will rather account for the conjugate by applying a factor of two, wherever necessary. Combinations of these SM particles build up the low-energy universe. While a majority of the visible matter in the universe is composed of the 1st generation fermions (e^-, v_e, u, d), there are three particle doublets for both leptons and quarks. Experimentally measured decay rates of μ and τ have indicated that weak interactions are equally strong for

all lepton flavours. This phenomenon is called lepton universality. An exception to lepton universality is generated by the Higgs field, as the Lepton-Higgs interaction strength produces unequal lepton masses $m_\tau > m_\mu > m_e$ [22].

Quarks interact with all 3 SM QFTs, charged leptons experience QED and the weak interaction, while neutrinos are charge-neutral and only experience the weak interaction. The QFTS are described using group theory, where QED is a U(1) local gauge symmetry, QCD is a SU(3) local gauge symmetry, While the weak interaction's charged-current corresponds to an invariance under SU(2) local phase transformations

$$\varphi(x) \to \varphi'(x) = \exp\left[i g_{\mathrm{W}}\, \boldsymbol{\alpha}(x) \cdot \mathbf{T}\right] \varphi(x). \tag{1}$$

Where $\mathbf{T} = \frac{1}{2}\boldsymbol{\sigma}$ are the three generators of the SU(2) group represented using Pauli matrices and $\alpha(x)$ are three functions representing the local phase at a point in spacetime. The requirement for local gauge invariance is only satisfied using three gauge fields $W_\mu^{1,2,3}$, which correspond to the three physical gauge bosons $W^\pm$ and Z. It is pragmatic to rewrite the wavefunction $\varphi(x)$ in terms of a weak isospin doublet, whose components differ by a single unit of electric charge. The leptons all have identical total weak isospin $I_W = +\frac{1}{2}$, but differing third component of Isospin magnitudes $I_W^3(\nu_l) = +\frac{1}{2}$ and $I_W^3(l^-) = -\frac{1}{2}$. Meanwhile, quarks have $I_W^3(u, c, t) = +\frac{1}{2}$, $I_W^3(d, s, b) = -\frac{1}{2}$. Hence, the weak isospin doublets are

$$\begin{pmatrix} \nu_e \\ e^- \end{pmatrix}_L, \begin{pmatrix} \nu_\mu \\ \mu^- \end{pmatrix}_L, \begin{pmatrix} \nu_\tau \\ \tau^- \end{pmatrix}_L \text{ for leptons,} \tag{2}$$

$$\begin{pmatrix} u \\ d \end{pmatrix}_L, \quad \begin{pmatrix} c \\ s \end{pmatrix}_L, \quad \begin{pmatrix} t \\ b \end{pmatrix}_L \text{ for quarks.} \tag{3}$$

Only left-handed chiral particle states and right-handed chiral antiparticle states contribute to the charged-current weak interaction. The weak charged-current mediated by the $W^\pm$ boson is responsible for transitions between two states in a doublet. This is the mechanism that we will primarily use in our particle decay calculations. Although HNLs are mostly sterile, they do mix with the light neutrino sector ν_e, ν_μ, ν_τ, through the active-sterile mixing matrix $|U_{\ell N}|^2$ which will be described in detail in section 2.1 below.

2.1 Heavy Neutral Leptons

As discussed in the section above, right-handed chiral neutrino states can not engage in any SM interactions. Therefore, we have no evidence for their existence. Nevertheless, as neutrinos are confirmed to be massive through neutrino oscillations data, they must have a corresponding mass term in the Lagrangian. In the SM, neutrino masses can be generated through an identical mechanism as for up-quarks, by using the conjugate Higgs doublet. After spontaneous symmetry breaking occurs, the gauge invariant Dirac mass term for a neutrino becomes

$$\mathcal{L}_D = -m_D\ (\overline{\nu_R}\ \nu_L + \overline{\nu_L}\ \nu_R). \tag{4}$$

However, neutrino masses are confirmed to be much lower than for the remaining fermions, which could mean that a separate mechanism for generating neutrino masses is responsible. As right-handed neutrinos and left-handed anti-neutrinos transform as singlets under SM

gauge transformations, any additional terms in the Lagrangian due to only these fields can be incorporated into the Lagrangian, without breaking the gauge invariance of the SM. Then left-handed antineutrinos $\bar{\nu}$, are included in the Lagrangian as CP conjugate fields

$$\psi^c = \hat{C}\hat{P}\psi = i\gamma^2\gamma^0\psi^*. \tag{5}$$

Therefore, the CP conjugate field for the right-handed neutrino ν_R^c, corresponds to the left-handed antineutrino. Hence, the Majorana mass term is

$$\mathcal{L}_M = -\frac{1}{2}M(\overline{\nu_R^c}\ \nu_R + \overline{\nu_R}\ \nu_R^c). \tag{6}$$

Such a majorana mass term demands for particles to couple directly to their corresponding antiparticles. As neutrinos are electrically neutral, they are not inherently forbidden from being their own antiparticles in the same manner as photon particles are their own antiparticles. The most general and renormalisable Lagrangian for neutrino masses merges the $\mathcal{L}_D$ and $\mathcal{L}_M$ terms. For just one light neutrino generation we have [23]

$$\mathcal{L}_{DM} = -\frac{1}{2}[m_D\overline{\nu_L}\nu_R + m_D\overline{\nu_R^c}\nu_L^c + M\overline{\nu_R^c}\nu_R] + h.c, \tag{7}$$

or in matrix form

$$\mathcal{L}_{DM} = -\frac{1}{2}(\overline{\nu_L}, \overline{\nu_R^c}) \begin{pmatrix} 0 & m_D \\ m_D & M \end{pmatrix} \begin{pmatrix} \nu_L^c \\ \nu_R \end{pmatrix} + h.c. \tag{8}$$

Where, h.c refers to the corresponding hermitian conjugate. Physical states for this implementation are obtained using the basis where the mass matrix is diagonal. The masses of the physical neutrino states are the eigenvalues of mass matrix A, and are acquired using the standard characteristic equation

$$\det(A - mI) = m^2 - Mm - m_D^2 = 0 \tag{9}$$

Therefore, the physical neutrinos masses are

$$m\pm = \frac{M \pm \sqrt{M^2 + 4m_D^2}}{2} = \frac{M \pm M\sqrt{1 + 4m_D^2/M^2}}{2}. \tag{10}$$

If $M \gg m_D$, then this equation may be approximated as

$$m\pm \approx \frac{1}{2}M \pm \frac{1}{2}\left(M + \frac{2m_D^2}{M}\right). \tag{11}$$

Therefore, the light neutrino state (ν) has a mass

$$|m_\nu| \approx \frac{m_D^2}{M}. \tag{12}$$

and the HNL mass (N) is

$$m_N \approx M. \tag{13}$$

The active-sterile neutrino mixing parameter

$$|U_{\ell N}| \sim \sqrt{\frac{m_D}{M}}, \tag{14}$$

generates the interaction between the HNL and active neutrino sectors [19]. Therefore, the neutrino gauge states contain a small contribution from HNLs, which results in indirect neutrino-like interactions for HNLs. The active-sterile mixing parameter ($|U_{\ell N}|^2$) matrix implementation for our three HNL flavours mixing with the light neutrino sector is given by

$$U = \begin{pmatrix} |U_{eN_1}|^2 & |U_{\mu N_1}|^2 & |U_{\tau N_1}|^2 \\ |U_{eN_2}|^2 & |U_{\mu N_2}|^2 & |U_{\tau N_2}|^2 \\ |U_{eN_3}|^2 & |U_{\mu N_3}|^2 & |U_{\tau N_3}|^2 \end{pmatrix}. \tag{15}$$

The regular HNL interaction rate can be derived from the active neutrino interaction rate Γ_ν using $\Gamma_N = |U_{\ell N}|^2 \Gamma_\nu$. This proposes that HNLs decouple at a higher temperature than active neutrinos [24]. The seesaw mechanism suggests that the m_D values for neutrinos are of comparable magnitude to the remaining fermions $\sim O(\text{GeV})$. In which case, the M term must be very large $M \sim 10^{11}$ GeV, so that the lighter of the physical ν states has a mass $m_\nu \sim 0.01$ eV, as required by neutrino oscillations data. Assuming the majorana mass term does actually exist, the seesaw mechanism suggests that for each neutrino generation ν_e, ν_μ, ν_τ, there is an extremely light neutrino of much lower mass than the remaining SM fermions and an extremely massive neutrino with mass $m_N \approx M$. In Figure 1 below, we can see the parameter space for the HNLs in the $(m_{N_2}, |U_{\mu N_2}|^2)$ plane. We can see the sections already ruled out by previous experiments (grey) and the coverage of upcoming experiments. It is this open parameter section, that we will be exploring in this study.

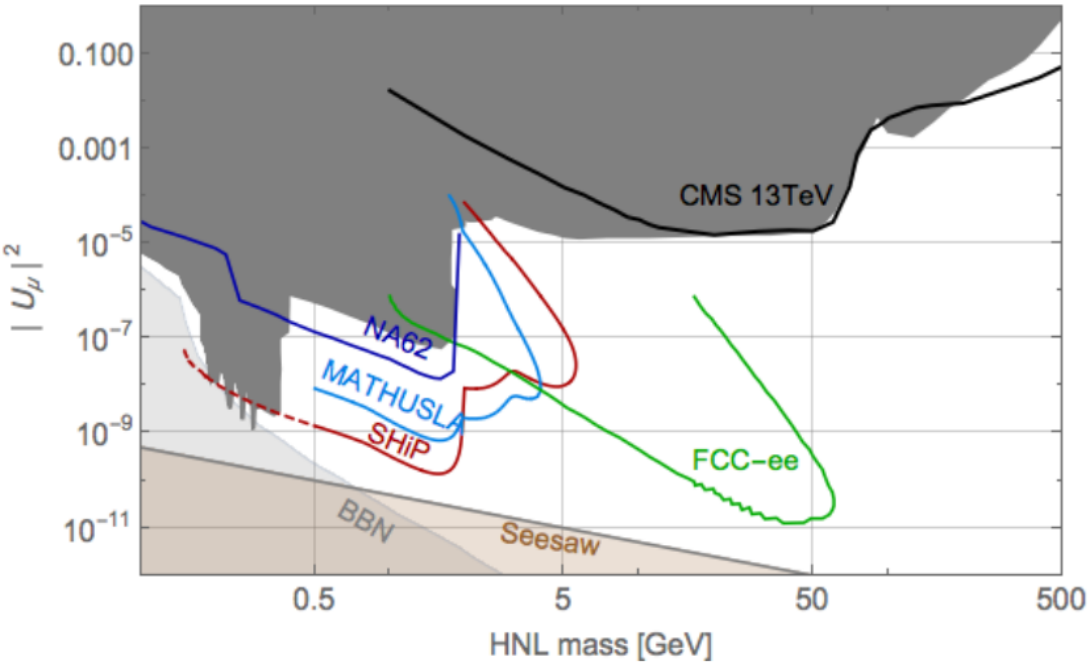

Figure 1: Plot obtained from [20], showing the existing limits and upcoming experimental searches for HNLs in the $(m_N, |U_\mu|^2)$. The grey section showcases the previously conducted experiments. The black solid line highlights recent bounds from the CMS 13 TeV run [25]. The sensitivity estimates from the prospective HNL experiments are based on [26] FCC-ee (green), [7] NA62 (dark blue), [27] SHiP (red) and [28] MATHUSLA@LHC (light blue). The primordial Big Bang Nucleosynthesis bounds on HNL lifetimes are from [29]. The seesaw section showcases which paremeters obey the seesaw relation $|U_\mu|^2 \sim m_\nu/M_N$. For this diagram the light neutrino mass substituted was $m_\nu = \sqrt{\Delta m^2_{\text{atm}}} \approx 0.05\text{eV}$ [8]

3 HNL Decays

3.1 Standard Model Channels

All HNL decays are mediated by the charged current (CC) or neutral current (NC) weak interactions. The decay widths shown below are written in the Dirac form, to account for the charge-conjugate channels of the majorana HNL, the relevent decay channels will be doubled, as shown in the discussion of the total decay width (3.11).

The impact of the Fermi contact theory approximation on the accuracy of the HNL decay widths will be worked out as a function of HNL mass following the theory developed in [21]. The Feynman rule for the exchange of a virtual W boson ($m_W = 80.4$ GeV) is

$$\frac{-i}{q^2 - m_W^2}\left(g_{\mu v} - \frac{q_\mu q_v}{m_W^2}\right). \tag{16}$$

For the limit $q^2 \ll m_W^2$, the $q_\mu q_v$ term is small and for lowest order calculations the $q_\mu q_v$ term

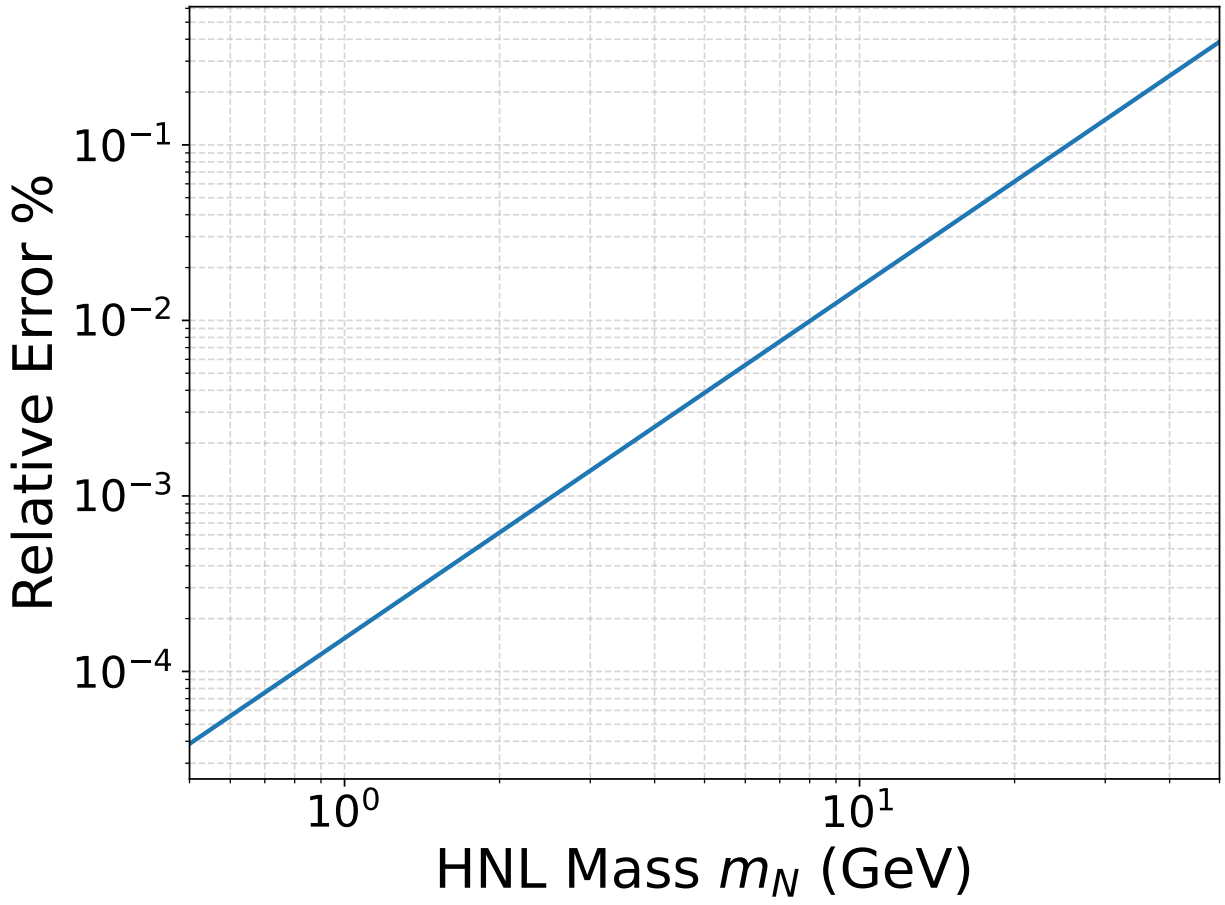

Figure 2: Relative error in the transition matrix element squared of the fermi contact theory approximation compared to the full weak propagator, expressed as a function of HNL mass m_N

do not measurably affect the matrix element squared hence we take the propagator to be

$$\frac{-ig_{\mu v}}{q^2 - m_W^2}. \tag{17}$$

Using this simplification we obtain the transition matrix element of the Feynman Rules for the weak interaction

$$M_{\text{Full}} = -\left[\frac{g_W}{\sqrt{2}}\bar{\psi}_3\frac{1}{2}\gamma^\mu(1-\gamma^5)\psi_1\right]\cdot\left[\frac{g_{\mu\nu}/m_W^2}{q^2-m_W^2}\right]\cdot\left[\frac{g_W}{\sqrt{2}}\bar{\psi}_4\frac{1}{2}\gamma^\nu(1-\gamma^5)\psi_2\right].$$

Where g_W is the weak coupling constant. The Fermi contact theory simplification uses

$$M_{\text{Full}} = \frac{1}{\sqrt{2}}G_F g_{\mu\nu}[\bar{\psi}_3\gamma^\mu(1-\gamma^5)\psi_1][\bar{\psi}_4\gamma^\nu(1-\gamma^5)\psi_2]. \tag{18}$$

Where $G_f = 1.166{\cdot}10^{-5}$ GeV is the fermi constant. Observables such as decays and scattering are calculated in terms of the transition probability, which squares the matrix elements. Now taking the ratio of these squared elements to work out the impact of the propagator

simplification

$$\left(\frac{M_{\text{Fermi}}}{M_{\text{Full}}}\right)^2 \approx \frac{m_W^2 - q^2}{m_W^2} = \left(1 - \frac{q^2}{m_W^2}\right)^2, \tag{19}$$

where $q^2 = t = (p_1 - p_3)^2 \approx m_N$ in our case of HNL N decay. Implementing this to obtain

$$\left(\frac{M_{\text{Fermi}}}{M_{\text{Full}}}\right)^2 = \left(1 - \frac{q^2}{m_W^2}\right)^2. \tag{20}$$

The relative error between the full propagator and Fermi contact theory approximation is

$$\left(\frac{M_{\text{Full}} - M_{\text{Fermi}}}{M_{\text{Full}}}\right)^2 = \left(1 - \left(1 - \frac{m_N^2}{m_W^2}\right)\right)^2, \tag{21}$$

which simplifies to

$$\left(\frac{M_{\text{Full}} - M_{\text{Fermi}}}{M_{\text{Full}}}\right)^2 = \left(\frac{m_N^2}{m_W^2}\right)^2. \tag{22}$$

In Figure 2, we can see this plotted over a range of HNL masses and hence see how the Fermi approximation becomes less accurate as we sample closer to the m_W boson mass. In our simulations we will consider mass ranges far below the m_W boson mass to minimise the impact of this approximation.

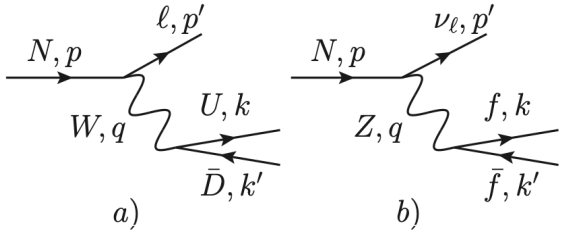

Figure 3: Feynman Diagrams for HNL decays mediated by the charged a) and neutral b) currents. Diagram obtained from [20].

Two simple diagrams shown in Figure 3, contribute to all decays. For the charged current-mediated decay (Figure 3(a)), the final particles (U, D) can be either a lepton pair $(\nu_\alpha, \ell_\alpha)$ or a pair of up and down quarks (u_i, d_j). For the neutral current-mediated decay case (Figure 3(b)) f is any fermionic particle. While the tree-level decay width into free quarks is not inherently physical for the mass range of interest, when modified by a QCD correction Δ_{QCD}, it provides a reasonable estimate for the full hadronic width at $m_N \gg \Lambda_{QCD}$, as described at the end of Section 3. For the $N \to \nu_\alpha \ell_\alpha^- \ell_\alpha^+$ and $N \to \nu_\alpha \nu_\alpha \bar{\nu}_\alpha$, both decay diagrams contribute, which causes interference (see section 3.3).

3.2 Charged-Current Mediated Decays

The general form of the charged current-mediated decays $N \to \ell_\alpha^- \nu_\beta \ell_\beta^+$, $\alpha \neq \beta$, and $N \to \ell_\alpha u_i \bar{d}_j$ is [30–33].

$$\Gamma(N \to \ell_\alpha^- U \bar{D}) = N_W \frac{G_F^2 m_N^5}{192\pi^3} |U_\alpha|^2 I(x_u, x_d, x_l), \tag{23}$$

f	C_1^f	C_2^f
u, c, t	$\frac{1}{4}\left(1 - \frac{8}{3}\sin^2\theta_W + \frac{32}{9}\sin^4\theta_W\right)$	$\frac{1}{3}\sin^2\theta_W\left(\frac{4}{3}\sin^2\theta_W - 1\right)$
d, s, b	$\frac{1}{4}\left(1 - \frac{4}{3}\sin^2\theta_W + \frac{8}{9}\sin^4\theta_W\right)$	$\frac{1}{6}\sin^2\theta_W\left(\frac{2}{3}\sin^2\theta_W - 1\right)$
$\ell_\beta, \beta \neq \alpha$	$\frac{1}{4}\left(1 - 4\sin^2\theta_W + 8\sin^4\theta_W\right)$	$\frac{1}{2}\sin^2\theta_W\left(2\sin^2\theta_W - 1\right)$
$\ell_\beta, \beta = \alpha$	$\frac{1}{4}\left(1 + 4\sin^2\theta_W + 8\sin^4\theta_W\right)$	$\frac{1}{2}\sin^2\theta_W\left(2\sin^2\theta_W + 1\right)$

Table 3: Neutral current-mediated decay coefficients C_1^f and C_2^f for fermionic particles. Table obtained from [20]

where $x_l = \frac{m_{\ell_\alpha}}{m_N}, x_u = \frac{m_U}{m_N}, x_d = \frac{m_D}{m_N}$. The pre-factor $N_W = 1$ for final state leptons and $N_W = N_c|V_{ij}|^2$ for final state quarks, where $N_c = 3$ is the number of quark colours and V_{ij} is the matching matrix element of the CKM matrix. The general function $I(x_u, x_d, x_l)$ details the corrections due to the finite masses of final-state fermions

$$I(x_u, x_d, x_l) \equiv 12\int_{(x_d+x_l)^2}^{(1-x_u)^2} \frac{dx}{x}(x - x_l^2 - x_d^2)(1 + x_u^2 - x)\sqrt{\lambda(x, x_l^2, x_d^2)\lambda(1, x, x_u^2)}, \tag{24}$$

where $\lambda(a, b, c)$ is the Kallen function [34] given by

$$\lambda(a, b, c) = a^2 + b^2 + c^2 - 2ab - 2ac - 2bc \tag{25}$$

3.3 Neutral Current-Mediated Decays $N \to \nu_\alpha f\bar{f}$

The decay width for the neutral current-mediated decay $N \to \nu_\alpha f\bar{f}$ is dependent on the flavour of final fermion. In the case of the charged lepton pair $l_\beta\bar{l}_\beta$ its values are different for the $\alpha \neq \beta$ and $\alpha = \beta$ cases, due to the impact of the charged current mediated diagrams in the latter case. However, the decay width may be expressed in general way as follows

$$\begin{aligned}\Gamma(N \to \nu_\alpha f\bar{f}) = N_Z\frac{G_F^2 m_N^5}{192\pi^3}|U_\alpha|^2 \cdot \Big[C_1^f\Big((1 - 14x^2 - 2x^4 - 12x^6)\sqrt{1-4x^2} \\ + 12x^4(x^4 - 1)L(x)\Big) + 4C_2^f\Big(x^2(2 + 10x^2 - 12x^4)\sqrt{1-4x^2} \\ + 6x^4(1 - 2x^2 + 2x^4)L(x)\Big)\Big],\end{aligned} \tag{26}$$

where $x = \frac{m_f}{m_N}$, $L(x) = \log\left[\frac{1-3x^2-(1-x^2)\sqrt{1-4x^2}}{x^2(1+\sqrt{1-4x^2})}\right]$ and $N_Z = 1$ for final state leptons or $N_Z = N_c$ for final state quarks. The values of C_1^f and C_2^f are given by (Table 3) above.

Pseudoscalar Meson	**Mass** (MeV)	**Decay Constant** (MeV)
$\pi^{\pm}$	139.6	130.2
$K^{\pm}$	493.7	155.6
$D^{\pm}$	1869.4	212
$D_s^{\pm}$	1968.3	249
$B^{\pm}$	5279	187
B_c	6274.47 [35]	434 [36]

Table 4: Mass and decay constants of pseudoscalar charged mesons used [31].

3.4 Decays into Light Neutrino States

In the case of exclusively light neutrino final states, only the neutral current can contribute and the decay width is

$$\Gamma(N \to \nu_\alpha \nu_\beta \bar{\nu}_\beta) = (1 + \delta_{\alpha\beta}) \frac{G_F^2 m_N^5}{768\pi^3} |U_\alpha|^2. \tag{27}$$

In this study we will evaluate hadronic final states for m_N values lower and higher than the Λ_{QCD} scale and consider the different assumptions made (exclusive hadronic channels vs quark + correction) and results obtained for both scenarios. At $m_N \lesssim \Lambda_{QCD}$ the quark pair primarily binds into a solitary meson. There are both charged current and neutral current-mediated mechanisms with a meson in the final state: $N \to \ell_\alpha h_{P/V}^+$ and $N \to \nu_\alpha h_{P/V}^0$, where $h_P^+(h_P^0)$ are charged (neutral) vector mesons. In the formulas listed below $x \equiv m_h/m_N$, $x_\ell = m_\ell/m_N$, f_h and g_h are the corresponding meson decay constants, θ_W is the Weinberg angle. $|V_{UD}|$ are the CKM matrix values [21].

$$\begin{pmatrix} |V_{ud}| & |V_{us}| & |V_{ub}| \\ |V_{cd}| & |V_{cs}| & |V_{cb}| \\ |V_{td}| & |V_{ts}| & |V_{tb}| \end{pmatrix} \approx \begin{pmatrix} 0.974 & 0.225 & 0.004 \\ 0.225 & 0.973 & 0.041 \\ 0.009 & 0.040 & 0.999 \end{pmatrix}.$$

3.5 Charged Pseudoscalar Meson Decays

The decay width to charged pseudo-scalar mesons ($\pi^{\pm}, K^{\pm}, D^{\pm}, D_s^{\pm}, B^{\pm}, B_c$) is

$$\Gamma(N \to \ell_\alpha^- h_P^+) = \frac{G_F^2 f_h^2 |V_{UD}|^2 |U_\alpha|^2 m_N^3}{16\pi} \left[(1 - x_\ell^2)^2 - x_h^2(1 + x_\ell^2)\right] \sqrt{\lambda(1, x_h^2, x_\ell^2)}. \tag{28}$$

The masses and decay constants used are shown in Table 4.

3.6 Neutral Pseudoscalar Meson Decays

The decay width to the pseudo-scalar neutral meson ($\pi^0, \eta, \eta', \eta_c$) is given by

$$\Gamma(N \to \nu_\alpha h_P^0) = \frac{G_F^2 f_h^2 m_N^3}{32\pi} |U_\alpha|^2 (1 - x_h^2)^2. \tag{29}$$

The masses and decay constants used are shown in Table 5.

Pseudoscalar Meson	**Mass** (MeV)	**Decay Constant** (MeV)
π^0	135	130
η	547.8	81.7
η'	957.8	-94.7
η_c	2979.6	237

Table 5: Mass and decay constants of pseudoscalar neutral mesons used [31].

Vector Meson	**Mass** (MeV)	**Decay Constant** (g_h) $(\text{GeV})^2$
$\rho^{\pm}$	775.8	0.162
$D^{*\pm}$	2010	0.535
$D_s^{*\pm}$	2112.1	0.650

Table 6: Charged Vector Mesons [20]

Vector Meson	**Mass** (MeV)	**Decay Constant** (g_h) $(\text{GeV})^2$	κ_h
ρ^0	775.26 [37]	0.162	$1 - 2sin^2\theta_W$
ω	782.59	0.153	$\frac{4}{3}sin^2\theta_W$
ϕ	1019.456	0.234	$\frac{4}{3}sin^2\theta_W - 1$
J/ψ	3096.916	1.29	$1 - \frac{8}{3}sin^2\theta_W$

Table 7: Neutral Vector Meson [20]

3.7 Charged Vector Meson decays

The HNL decay width into charged vector mesons ($\rho^{\pm}, D^{\pm *}, D_s^{\pm *}$) is given by

$$\Gamma(N \to \ell_\alpha h_V^+) = \frac{G_F^2 g_h^2 |V_{UD}|^2 |U_\alpha|^2 m_N^3}{16\pi m_h^2} \left((1-x_\ell^2)^2 + x_h^2(1+x_\ell^2) - 2x_h^4\right) \sqrt{\lambda(1, x_h^2, x_\ell^2)}. \quad (30)$$

The masses and decay constants used are shown in Table 6.

3.8 Neutral Vector Meson Decays

For decays into neutral vector meson ($\rho^0, a_1^0, \omega, \phi, J/\psi$) the value depends on the quark composition of the meson. Hence, we add a dimensionless κ_h factor to the meson decay constant. The decay width is

$$\Gamma(N \to \nu_\alpha h_V^0) = \frac{G_F^2 \kappa_h^2 g_h^2 |U_\alpha|^2 m_N^3}{32\pi m_h^2} (1+2x_h^2)(1-x_h^2)^2. \quad (31)$$

The masses, decay constants and κ_h used are shown in Table 7.

3.9 QCD Correction

HNLs can decay into multi-hadronic final states for $m_N > 2m_\pi$. These channels quickly become very difficult to model accurately. However they can be approximated to relatively well by calculating the HNL decays into quarks and applying a QCD correction factor to the

decay width

$$\Gamma_{\text{Corrected}} = \Gamma_{\text{Quarks}}(1 + \Delta_{QCD}) \tag{32}$$

where

$$\Delta_{\text{QCD}} = \frac{\alpha_s}{\pi} + 5.2\frac{\alpha_s^2}{\pi^2} + 26.4\frac{\alpha_s^3}{\pi^3} \tag{33}$$

and $\alpha_s = \alpha_s(m_N)$ is the strong force running coupling. We use this Δ_{QCD} correction to the HNL decay to quark channels instead of the individual meson channel for $m_N > 2$GeV values as this is when the quark + Δ_{QCD} channel becomes dominant, as will be shown in Figure 5 below. The value of Δ_{QCD} is inversely proportional to the heavy neutrino mass m_N. For completeness I will now show the derivation of $\alpha_s(m_N)$.

[38] In Perturbative QCD (pQCD) predictions for physical observables are shown in terms of the renormalised coupling $\alpha_s(\mu_R^2)$, a function of the (unphysical) renormalisation scale μ_R. Taking μ_R near to the scale of the momentum transfer Q in a given mechanism, then $\alpha_s(\mu_R^2 \simeq Q^2)$ is representative of the effective strength of the strong interaction in that mechanism. This coupling satisfies the following renormalisation group equation (RGE)

$$\mu_R^2 \frac{d\alpha_s}{d\mu_R^2} = \beta(\alpha_s) = -\left(b_0\alpha_s^2 + b_1\alpha_s^3 + b_2\alpha_s^4 + \cdots\right), \tag{34}$$

where $b_0 = \frac{11C_A - 4n_f T_R}{12\pi} = \frac{33-2n_f}{12\pi}$ is the 1-loop β-function coefficient, and n_f is the number of quark flavours. The minus sign is the source of "asymptotic freedom" [39,40] (why the strong coupling becomes small for processes involving large momentum transfers). The pQCD theory is strongly interacting at momentum transfer scales around and below 1GeV. The coupling can be isolated into a more useful form by solving this differential equation

$$\mu_R^2 \frac{d\alpha_s}{d\mu_R^2} = -b_0\alpha_s^2. \tag{35}$$

In our model the variable parameter is the sterile neutrino mass, hence in the implementation we will integrate from a reference scale Λ_{QCD} up to m_N^2,

$$\int_{\alpha_s(\Lambda^2)}^{\alpha_s(m_N^2)} \frac{d\alpha_s}{\alpha_s^2} = -b_0 \int_{\Lambda^2}^{m_N^2} \frac{d\mu_R^2}{\mu_R^2}, \tag{36}$$

to obtain

$$\left[-\frac{1}{\alpha_s}\right]_{\alpha_s(\Lambda^2)}^{\alpha_s(m_N^2)} = -b_0 \left[\ln\left(\mu_R^2\right)\right]_{\Lambda^2}^{m_N^2}. \tag{37}$$

Evaluating the integral at the limits results in

$$-\frac{1}{\alpha_s(m_N^2)} + \frac{1}{\alpha_s(\Lambda^2)} = -b_0\left(\ln\left(m_N^2\right) - \ln\left(\Lambda^2\right)\right). \tag{38}$$

The QCD scale, Λ_{QCD}, is defined as the energy at which the coupling becomes infinite, i.e., $\alpha_s(\Lambda^2) \to \infty$. Therefore, the term $\frac{1}{\alpha_s(\Lambda^2)} \to 0$. The equation simplifies significantly:

$$-\frac{1}{\alpha_s(m_N^2)} = -b_0 \ln\left(\frac{m_N^2}{\Lambda^2}\right). \tag{39}$$

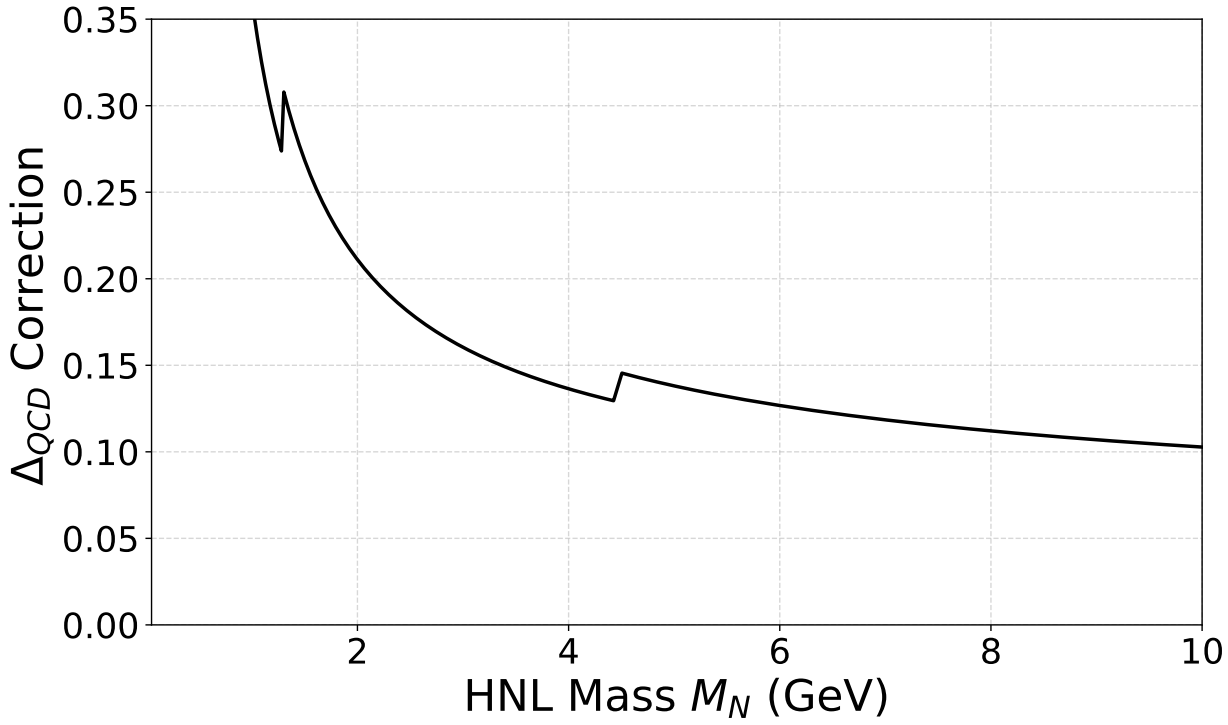

Figure 4: Correction factor Δ_{QCD} as a function of the heavy neutrino mass m_N.

Canceling the negative signs and taking the reciprocal of both sides yields the solution

$$\alpha_s(m_N^2) = \frac{1}{b_0 \ln(m_N^2/\Lambda^2)}, \tag{40}$$

where the one-loop coefficient b_0 as:

$$b_0 = \frac{33 - 2n_f}{12\pi}. \tag{41}$$

Here n_f refers to the number of quark flavours active for the energy regime and in Figure 4 we can clearly see when the charm and bottom flavours are activated via the sharp increases in the Λ_{QCD} value at the charm quark mass (1.3 Gev) and bottom quark mass (4.5 GeV).

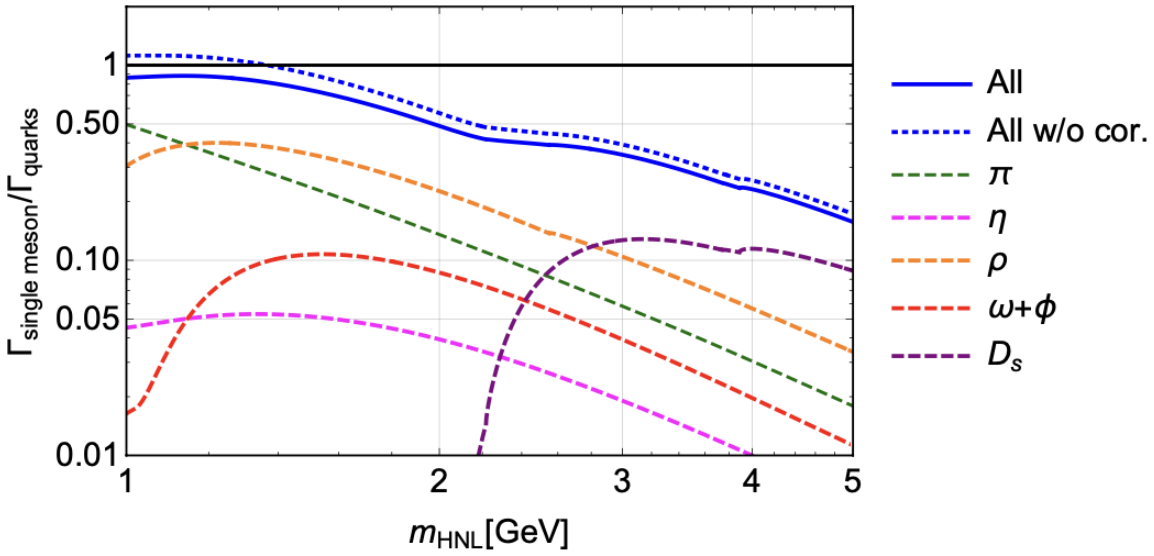

Figure 5: HNL decay widths into summed and individual single meson channels, divided by the total decay width into quarks+ Δ_{QCD} as a function of the heavy neutrino mass (m_N). The blue solid curve shows the total single meson channels divided by the total quark + Δ_{QCD} channel. The blue dotted curve shows the total single meson channels divided by the total quark channels without the Δ_{QCD} correction. The rest of the dotted lines show the decay widths into the specific single meson species divided by the total quark width + Δ_{QCD} correction. Image obtained from [20].

Figure 5 shows that the decay width into Quarks + Δ_{QCD} begins to dominate over the decay width into single mesons at $\sim$ 2 GeV, hence in this study's simulations we will dynamically switch between the two regimes.

- Single Meson decays for $m_N < 2$ GeV
- Quarks+QCD correction for $m_N > 2$ GeV.

In the single-meson channels detailed in the section above, we incorporated decays which include the ρ meson. Through this we in effect include all the two-pion channels $N \to \pi^+\pi^0\ell^-$ for $m_N > m_\rho$. [20] have verified through direct computation of $N \to \pi^+\pi^0\ell^-$ that they coincide with the $N \to \rho^+\ell^-$ for all HNL masses of interest. Additionally, while the channel to two pions is available for $2m_\pi < m_N < m_\rho$, its contribution is negligibly small and hence, is ignored for the following discussion. [31] show that for a Majorana HNL with mass m_N, the lowest-order weak decays fall into two distinct kinematic regimes.

- Three-body decays via off-shell W/Z bosons. In terms of the Fermi contact interaction the decay width can be written as

$$\Gamma_{3-\text{Body}} \sim G_f^2 m_N^5 |U_{\ell N}|^2 \tag{42}$$

- Two-body decays into an on-shell boson plus a lepton.

$$N \to \ell^\pm W^\mp, N \to \nu Z, N \to \nu H. \tag{43}$$

Here H is the Higgs boson. With a decay width of

$$\Gamma_{\text{Two-Body}} \sim g'^2 m_N \tag{44}$$

While in principle both scenarios must be accounted for, at low masses $\ll m_{W/Z}$, the three-body decay dominates, and the two-body decay only becomes significant near the W boson mass (80.4 GeV). Our simulation will not consider mass ranges high enough for two body decays to be significant, so they will be omitted in the result, but in principle they need to be taken into account, particularly if the model is to be extended to higher masses.

3.10 Deppisch ALP Extension

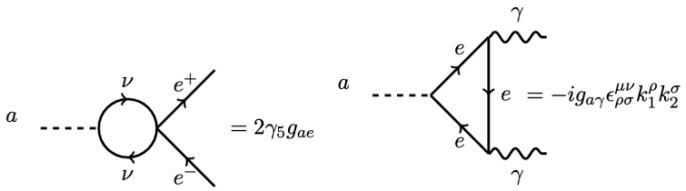

Figure 6: ALP effective couplings to electrons (left) and photons (right). Image obtained from [19]

In addition to the SM decays, we will incorporate the model proposed by [19], which includes a very low mass pseudo-scalar axion-like particle (ALP), that exclusively couples to the HNL in an un-broken SM and therefore, the ALP mass is not rigidly constrained to the QCD transition scale Λ_{QCD}. An interaction between the ALP and active neutrinos ν_α is instigated via the miniscule active-sterile mixing parameter $|U_{\ell N}|^2$. This mixing would open up the potential for an exotic decay channel

$$\sum_{\alpha=e,\mu,\tau} \Gamma_{N_i \to a\nu_\alpha} = \frac{|U_{\ell_\alpha N_i}|^2 m_{N_i}^3}{4\pi f_a^2} \sqrt{1 + \left(\frac{m_a}{m_{N_i}}\right)^2} \left[1 - \left(\frac{m_a}{m_{N_i}}\right)^2\right]^{\frac{3}{2}}. \tag{45}$$

This interaction would need the ALP to be long-lived $\tau_a > 10^4$ s, to avoid increasing the temperature of the primordial neutrino bath, which would delay neutrino decoupling and BBN. For $m_a \lesssim 1$ keV, the only allowed decays are $a \to \gamma\gamma$ and $a \to \nu\nu$. However, the $\gamma\gamma$ decay is strongly suppressed as a two-loop process. Therefore, the tree level $a \to \nu\nu$ decay is absolutely dominant.

$$\Gamma^{a \to \nu_\alpha \nu_\alpha} = \frac{1}{f_a^2} \frac{m_{N_\alpha}^2 m_a |U_{\ell N_\alpha}|^4}{2\pi} \sqrt{1 - \frac{4m_{\nu_\alpha}^2}{m_a^2}} \left(1 - \frac{2m_{\nu_\alpha}^2}{m_a^2}\right) \simeq \frac{m_{N_\alpha}^2 m_a U_{\ell N_\alpha}^4}{2\pi f_a^2}. \tag{46}$$

ALP properties are mainly constrained via their interactions with electrons and photons. These, originate from the $aNN \to a\nu\nu \to aee \to a\gamma\gamma$ coupling, which occurs at 1-loop and 2-loop levels, as shown in Figure 6. The effective coupling strengths of the ALPs with

electrons and photons are

$$g_{ae} \approx \frac{\sqrt{2} G_F g_{aN} |U_{eN}|^4 m_e m_N}{16\pi^2} = \frac{\sqrt{2} G_F |U_{eN}|^4 m_e m_N^2}{16\pi^2 f_a} \tag{47}$$

$$g_{a\gamma} \approx \frac{e^2 g_{ae}}{2\pi^2 m_e} \left(1 + \frac{1}{12}\frac{m_a^2}{m_e^2}\right) = \frac{\sqrt{2} e^2 G_F |U_{eN}|^4 m_N^2}{32\pi^4 f_a} \left(1 + \frac{1}{12}\frac{m_a^2}{m_e^2}\right), \tag{48}$$

where $g_{aN} = \frac{m_N}{f_a}$.

3.11 Total decay width and branching ratios

Summing this new ALP decay channel and all of the allowed SM decay channels for the HNL, we obtain the total decay width in our two regimes. In the exclusive hadronic range $m_N < 2\text{GeV}$ we include the hadronic decay channels into single meson states. For HNL flavour $N_i = 1, 2, 3$

$$\begin{aligned}\Gamma_{N_i} = 2 \sum_{\alpha=e,\mu,\tau} \Bigg[& \sum_{\beta\neq\alpha} \Gamma(N_i \to \ell_\alpha^- \nu_\beta \ell_\beta^+) + \sum_{\beta=e,\mu,\tau} \Gamma(N_i \to \nu_\alpha \ell_\beta^- \ell_\beta^+) \\ & + \sum_{\beta=e,\mu,\tau} \Gamma(N_i \to \nu_\alpha \nu_\beta \bar{\nu}_\beta) + \sum_{P^+_{\text{Allowed}}} \Gamma(N_i \to \ell_\alpha^- P^+) \\ & + \sum_{P^0_{\text{Allowed}}} \Gamma(N_i \to \nu_\alpha P^0) + \sum_{V^+_{\text{Allowed}}} \Gamma(N_i \to \ell_\alpha V^+) \\ & + \sum_{V^0_{\text{Allowed}}} \Gamma(N_i \to \nu_\alpha V^0) + \Gamma(N_i \to a\nu_\alpha) \Bigg].\end{aligned} \tag{49}$$

In the inclusive hadronic range $> 2\text{GeV}$, the single meson channels are replaced with the quark + Δ_{QCD} correction decay channels

$$\begin{aligned}\Gamma_{N_i} = 2 \sum_{\alpha=e,\mu,\tau} \Bigg[& \sum_{\beta\neq\alpha} \Gamma(N_i \to \ell_\alpha^- \nu_\beta \ell_\beta^+) + \sum_{\beta=e,\mu,\tau} \Gamma(N_i \to \nu_\alpha \ell_\beta^- \ell_\beta^+) \\ & + \sum_{\beta=e,\mu,\tau} \Gamma(N_i \to \nu_\alpha \nu_\beta \bar{\nu}_\beta) \\ & + (1 + \Delta_{\text{QCD}(m_{N_i})}) \Bigg[\sum_{u_i,d_j} \Gamma(N_i \to \ell_\alpha^- u_i \bar{d}_j) + \sum_{\text{Allowed q}} \Gamma(N_i \to \nu_\alpha q\bar{q}) \Bigg] \\ & + \Gamma(N_i \to a\nu_\alpha) \Bigg].\end{aligned} \tag{50}$$

4 Application to Cosmology

The ensuing theoretical discussion follows [41]. The early universe can be considered a hot gas of weakly interacting particles, and thus it is prudent to describe its properties in terms of statistical mechanics. The particle species densities will be derived using probability distribution functions. Considering the early universe to be in thermal equilibrium, these functions are given by the Fermi-Dirac distribution for fermions and the Bose-Einstein distribution for bosons

$$f(p,T) = \frac{1}{e^{(E(p)-\mu)/T} \pm 1}, \tag{51}$$

with + sign for fermions and - sign for bosons, where μ is the chemical potential. This microscopic view of the gas is related to its macroscopic behaviour by summing over all possible momentum states of the particles scaled by their probabilities. Hence, the number density of the particles in the gas is given by

$$n = \sum_p f(p,T). \tag{52}$$

To convert this sum over states into an integral over a continous momentum variable $\mathbf{p}$ requires the density of states, which is derived by treating the gas as a quantum system. In momentum space a gas of particles with internal degrees of freedom g has the density of states in natural units

$$\frac{g}{h^3} = \frac{g}{(2\pi)^3}. \tag{53}$$

Combining the above we obtain the number density of particles

$$n(T) = \frac{g}{(2\pi)^3} \int d^3p \; f(p,T). \tag{54}$$

Neutrinos are considered to have two internal degrees of freedom each $g = 2$ [41]. While left handed neutrinos $(\nu_e, \nu_\mu, \nu_\tau)$ are readily observed in nature, right-handed neutrinos have not, and it has long been assumed that they simply do not exist. However as we now know that neutrinos are not massless, which forbids the simple explanation above. There are two types of masses that the neutrinos can have, a Dirac mass or a Majorana mass. If it is a majorana particle , the neutrino is its own particle, like the photon and instead of one degree of freedom from the particle and antiparticle, we have 2 degrees of freedom from each neutrino and zero contribution from antineutrinos. The neutrino can be its own antiparticle like the photon as it has zero charge. If the neutrino had a Dirac mass instead, we would have to count 2 internal degrees of freedom for both the particle and the antiparticle, for a total of 4. This is incompatible with measurements from BBN. This result suggests that either neutrinos are majorana particles or half of the dirac neutrinos internal degrees of freedom decoupled in the very early universe through some unknown mechanism and their energy density was diluted, so that these additional two degrees of freedom made an insignificant impact by the time of BBN. Such models do exist, however this study will focus exclusively on exploring the Majorana scenario.

Each particle species has its own distribution function f_i and therefore, its own densities and pressures n_i, ρ_i, P_i. Species which are in thermal equilibrium share a common temperature $T_i = T$. Hence, the densities and pressure can only vary because of differences in

their masses and chemical potentials. However, at early times the chemical potentials of all particle species are much lower than the temperature $|\mu_i| \ll T$, and will therefore be ignored for this study. Using $\mu = 0$ and the on-shell relation $E(p) = \sqrt{p^2 + m^2}$ we get

$$n = \frac{g}{2\pi^2} \int_0^\infty dp \; \frac{p^2}{\exp[\sqrt{p^2 + m^2/T}] \pm 1}. \tag{55}$$

Defining the dimensionless variable $z = m/T$ and $\zeta = p/T$, hence the equation can be expressed as

$$n = \frac{g}{2\pi^2} T^3 I_\pm(z), \quad I_\pm(z) = \int_0^\infty d\zeta \frac{\zeta^2}{\exp[\sqrt{\zeta^2 + z^2}] \pm 1}. \tag{56}$$

In the relativistic limit where temperatures are much greater than the particle mass, we take the limit $z \to 0$ and our integral simplifies to

$$I_\pm(0) = \int_0^\infty d\zeta \frac{\zeta^2}{e^\zeta \pm +1}. \tag{57}$$

By expanding the denominator as a geometric series the $I_\pm(0)$ can be approximated as a Riemann zeta function with

$$I_-(0) = 2\zeta(3) \quad \text{for bosons,} \tag{58}$$

$$I_+(0) = \frac{3}{4} I_-(0) \quad \text{for fermions.} \tag{59}$$

Thus we finally get the number densities of particle species in the relativistic limit

$$n = \frac{\zeta(3)}{\pi^2} \; gT^3 \quad \text{for bosons,} \tag{60}$$

$$n = \frac{3}{4} \frac{\zeta(3)}{\pi^2} \; gT^3 \quad \text{for fermions.} \tag{61}$$

In the non-relativistic limit the temperatures are well below the particle mass and we take the limit $x \gg 1$ and the integral $I_\pm(z)$ is the same for both bosons and fermions.

$$I_\pm(z) \approx \int_0^\infty d\zeta \frac{\zeta^2}{e^{\sqrt{\zeta^2 + z^2}}}. \tag{62}$$

A majority of the contribution to the integral results from the $\zeta \ll z$ regime and through a taylor expansion of the square root in the exponential to the lowest order in ζ we obtain,

$$I_\pm(x) \approx \int_0^\infty d\zeta \frac{\zeta^2}{e^{z + \zeta^2/(2z)}} = e^{-z} \int_0^\infty d\zeta \; \zeta^2 e^{-\zeta^2/(2z)} = (2z)^{3/2e^{-z}} \int_0^\infty d\zeta \; \zeta^2 e^{-\zeta^2} \tag{63}$$

once the standard gaussian integral is evaluated, this expression simplifies down to

$$I_\pm(z) = \sqrt{\frac{\pi}{2}} z^{\frac{3}{2}} e^{-z} \tag{64}$$

As expected from probability distribution functions

$$\frac{I_{\pm}(z)}{I_{-}(0)} \approx 0.5 z^{3/2} e^{-z} \ll 1. \tag{65}$$

which shows that massive particles are exponentially rare at low temperatures. Bringing this integral back into the number density of particle species to obtain the number density of the non-relativistic gas

$$n_{X_{eq}} = g \left(\frac{m^2}{2\pi z}\right)^{\frac{3}{2}} e^{-z}. \tag{66}$$

However due to the expansion of the universe, a more intuitive measure of relative abundances is given through the comoving yield

$$Y_X = \frac{n_x}{s}, \tag{67}$$

where s is the entropy density

$$s = \frac{2\pi^2}{45} g_\star T^3. \tag{68}$$

where g_* is the relativistic degrees of freedom. The values used are listed in the table below.

Event	**Temperature**	g_{*n}	g_{*e}	g_{*p}	g_{*s}
Annihilation of $t\bar{t}$ quarks	$<$ 173.3 GeV	95.5	106.75	106.75	106.75
Annihilation of Higgs boson	$<$ 125.6 GeV	86.5	96.25	96.25	96.25
Annihilation of Z^0 boson	$<$ 91.2 GeV	85.5	95.25	95.25	95.25
Annihilation of W^+W^- bosons	$<$ 80.4 GeV	82.5	92.25	92.25	92.25
Annihilation of $b\bar{b}$ quarks	$<$ 4190 MeV	76.5	86.25	86.25	86.25
Annihilation of $\tau^+\tau^-$ leptons	$<$ 1777 MeV	67.5	75.75	75.75	75.75
Annihilation of $c\bar{c}$ quarks	$<$ 1290 MeV	64.5	72.25	72.25	72.25
QCD transition†	150–214 MeV	55.5	61.75	61.75	61.75
Annihilation of $\pi^+\pi^-$ mesons	$<$ 139.6 MeV	15.5	17.25	17.25	17.25
Annihilation of π^0 mesons	$<$135.0 MeV	13.5	15.25	15.25	15.25
Annihilation of $\mu^+\mu^-$ leptons	$<$105.7 MeV	9.5	10.75	10.75	10.75
Neutrino decoupling	$<$800 keV	6.636	6.863	6.863	7.409
Annihilation of e^+e^- leptons	$<$511.0 keV	3.636	3.363	3.363	3.909

Table 8: Relativistic Degrees of Freedom in the Early Universe, table obtained from [42].

These values are calculated using lattice QCD and hence can vary depending on the model. A plot of the relativistic degrees of freedom parameterised in terms of $z = m_N/T$ can be seen in Figure 7 below. As $z = m_N/T$ varies over a wide range of magnitudes, they are sampled using np.logspace, which returns values spaced evenly over a $\log_{10}$ scale.The thermally averaged interaction density $\gamma_{X\to Y}$, defined as

$$\gamma_{X\to Y} = \langle \sigma_{X\to Y} v | \sigma_{X\to Y} v \rangle \, n_X^{eq,2} = \langle \Gamma_{X\to Y} | \Gamma_{X\to Y} \rangle \, n_X^{eq}, \tag{69}$$

where n_X^{eq} is the number density of species X while on thermal equilibrium. The thermally

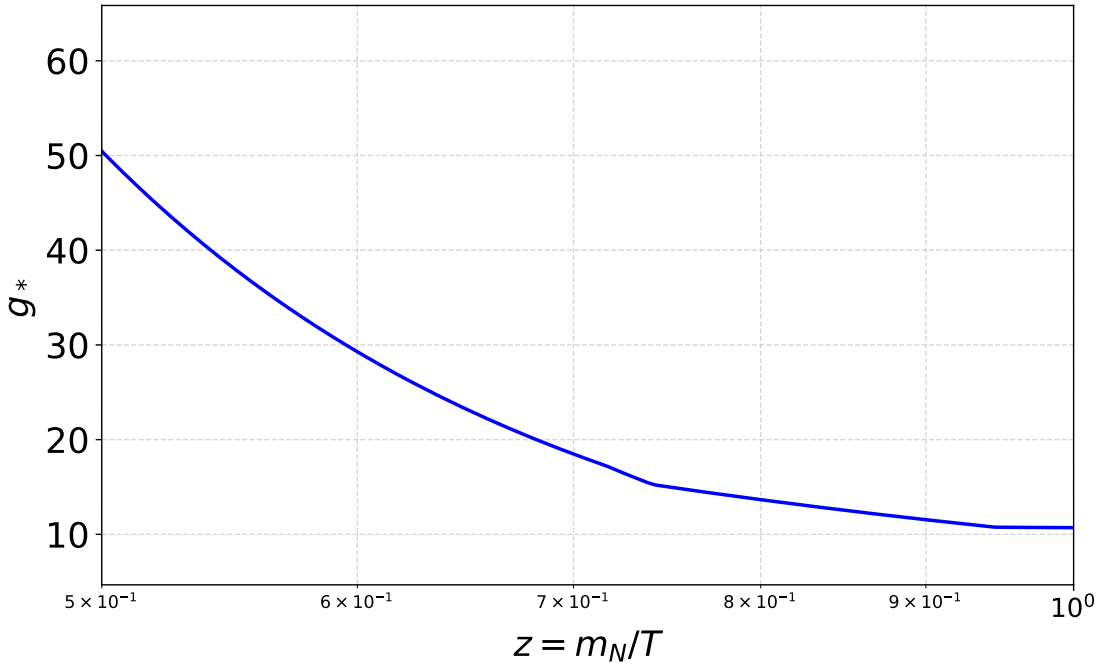

Figure 7: Relativistic Degrees of Freedom as a function of temperature T, parameterised using $z = m_N/T$

.

averaged decay width density is defined as

$$\gamma_{X \to Y_1 ....} = n_X^{eq}(z) \frac{K_1(z)}{K_2(z)} \Gamma_X, \tag{70}$$

where $z = \frac{m_X}{T}$, Γ_X is the zero-temperature decay width of particle X, and $K_{1(2)}(z)$ are the Bessel functions of the first (second) kind.

The universe is expanding [43]. Hence, in the past it was denser and hotter, particles were interacting frequently and the universe was in thermal equilibrium. In this study we are interested in the interactions, equilibrium densities of particle species, hence for clarity it will be prudent to consider the universe's evolution over temperature instead of time. It is useful to set Boltzmann's constant to unity, $k_B = 1$, and calculate temperature in units of energy.

$$1\ eV \approx 1.60\ x\ 10^{-19} J \approx 1.16\ x\ 10^4 K. \tag{71}$$

5 Implementation in Python

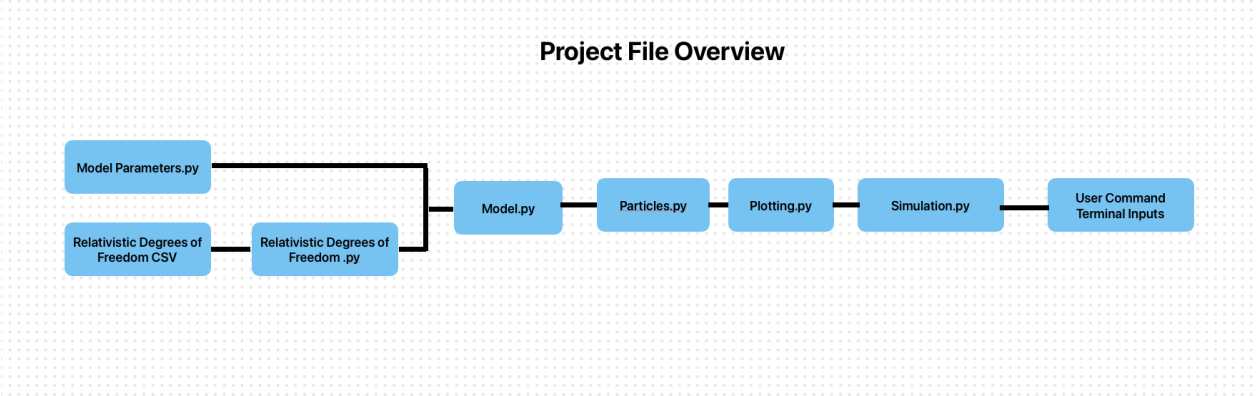

Figure 8: High-Level overview of the relationship between files in this python engine.

This section describes the structure and functionality of the Python framework developed to implement the GeV-scale HNL phenomenology presented in [20]. The full codebase is publicly available on Github [44]. The ability to extend this code to additional exotic particles and decay channels was a core design priority as is demonstrated by the implementation of the ALP and its dominant decay, first introduced in [19]. The codebase is organised into modular python files each encapsulating a specific role as shown in Figure 8. The 'Model Parameters' and 'Relativistic Degrees of Freedom' modules set the physical parameters of the scenario, which is then initialised in the 'Model.py' file. The Model.py file contains a class: Model, which is called inside the Particles file to calculate the decay widths defined within each particle species class. These defined particle species and decays are then imputed into the Plotting.py file, where the decays and other calculations are looped over a range of parameters. The results of these analyses are then called by the various scenario cases in the Simulation.py file. This simulation file defines the required terminal user commands, through which the user executes the simulation. In the subsections below the function of each file in the engine is described, along with explanations for particular design choices.

5.1 Particles.py

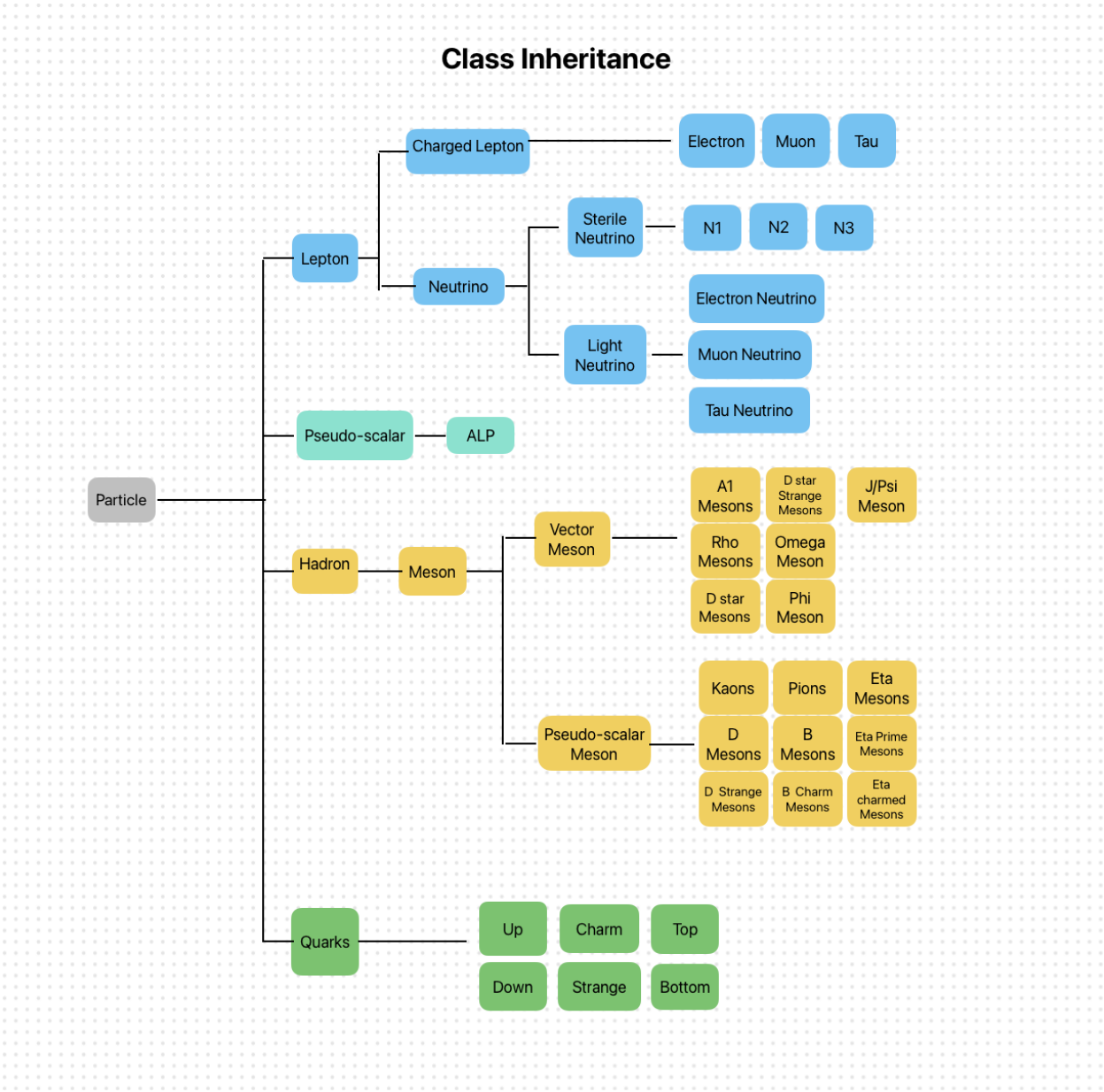

Figure 9: Diagram showing the branching inheritance of every particle species defined in this engine.

The particles were defined with an object-oriented programming approach in mind. Where new classes of particles are created based on an existing class (superclass). The new class (subclass) inherits the attributes and properties of the superclass, allowing for the reusability of code and relating particles to each other in a user-friendly way. The parent class simply called 'Particle' has only one parameter (mass). As shown in Figure 9 above, the quark, hadrons, Pseudoscalar and Lepton subclasses all inherit directly from the 'Particle' superclass. Each adding their own properties as will be described in the text below. These subclasses split into further subclasses to implement specific particles and their properties. Subclasses were implemented as widely as possible, in a way that ensured that decay width equations

could not possibly take the incorrect particle class as an input. Some key properties of the Particle file implementation are

- **Extendability**
  - New particles and decay channels can be added by subclassing Particle (or appropriate intermediary base class) and extending the SterileNeutrino.calculate_decay_width decay logic.
- **Modularity**
  - Phase-space integrals, mixing, correction factors, etc, are all localised within the particle classes, keeping the plotting and simulation files as free from detailed formulae as possible.
- **Performance**
  - Kinematics: The first step of a partial decay width calculation is to run a kinematic check, to see if the decay channel is possible for the current parameter values. This ensures that computational resources use is as efficient as possible.
  - The total decay width caches for the ALP and Sterile Neutrino prevent repeated calculation of functions for identical kinematic points.

The crucial mechanism to understand in this Particles module can be summarised as follows

- Particle species are defined as unique subclasses.
- Lists of theoretically possible decay channels are created in process specific list function (e.g. charged vs neutral current decay lists).
- These lists are fed into specific functions (e.g. leptonic and hadronic decay width calculators) which check if the process is kinematically and physically possible and then calculates the decay width.
- A function sums all of these partial decay width calculations to obtain a total decay width for the particle species.
- A function divides the partial decay width of interest by the total decay width to obtain the branching ratio for a decay channel of interest.

Now we will discuss the specific details of how the Particles module operates for completeness.

- **Particle**: This is the parent class. It stores only a single attribute: mass [GeV].
- **Lepton, Quark, Pseudoscalar and Hadron** are the first subclasses which inherit from the Particle parent class and either add their own specific properties (Quarks and Pseudoscalar) or add nothing and are used for clarity to later hold further specific subclasses which do add new properties(Hadron and Leptons).

- **Quark** adds the 'flavour' property string for the six quark flavours (up,down,charm, strange,top,bottom) and sets the mass of each. The subclass also specifies whether the flavour'is_up_type' (i.e. up, charm, top), which is used to validate user-defined decay channels as only certain quark pairs are physically allowed.

- **Pseudoscalar** introduces the pseudoscalar decay constant property. This class will be the parent class of our specific ALP.

- **Lepton** This class acts as a container which will be the parent class of the neutrino and charged lepton subclasses.

- **Hadron** This class also acts as a container for the Vector and Pseudoscalar meson subclasses.

  Now the above subclasses are further split into the specific subclasses which are used in the decay width calculations.

- **Meson** inherits from Hadron and introduces the properties: quark content and charge.

- The **PseudoscalarMeson** subclass inherits from the Meson class and introduces the decay constant parameter f. Two further subclasses derive from the Pseudoscalar Meson class

  - **Charged Pseudoscalar Meson**, with the specific particle subclasses ($\pi^{\pm}$, $K^{\pm}$, $D^{\pm}$, $D_s^{\pm}$, $B^{\pm}$, $B_c^{\pm}$)
  - **Neutral Pseudoscalar Meson**, with the specific particle subclasses ($\pi^0, \eta, \eta', \eta_c$)

- The **Vector Meson** subclass inherits from Meson and has two further subclasses

  - The **Charged Vector Meson** subclass introduces the vector decay constant g. The specific particle subclasses are ($\rho^{\pm}, D^{*\pm}, D_s^{*\pm}$)
  - The **Neutral Vector Meson** subclass introduces the vector decay constant g and the κ factor. The specific particle subclasses of which are ($\rho^0, \omega, \phi, J/\psi$).

-

- The **ALP** subclass inherits from the pseudoscalar class and contains the specific mass and decay constant parameters of the ALP. It also contains the ALP decay implementation which is defined in detail as follows

  - **ALP_channels(model)**: Holds all the ALP channels to allow for future extension of the model by adding further decay channels.
  - **calculate_decay_width(outgoings,model):**
    - Verifies the validity of the kinematics and that the two final state neutrinos have the same flavour.
    - model.get_U_alpha(sterile,charged_lepton): Retrieves the active-sterile mixing parameter $|U_{\ell N|^2}$ corresponding to the light neutrino flavour.
    - Evaluates the decay width formula $\Gamma_{a\to\nu\nu}$

- **get_total_decay_width(model)**: Caches and sums over all three channels using ALP_channels and calculate_decay_width.

- The **Charged Lepton** subclass inherits from the lepton subclass, and is further split into the specific particle subclasses with their mass values set.
  - **Electron**
  - **Muon**
  - **Tau**

- The **Neutrino** subclass which inherits from lepton and is used as a container for the SterileNeutrino (HNL) and light neutrino (ν_α) subclasses.

- The **light neutrino** subclass implements the type 1 seesaw mechanism by taking the active sterile mixing parameter from the Model module (defined in Model.py section below). This is used to dynamically set the light neutrino mass for each flavour (e, μ, τ) as follows $m_{\nu_\alpha} = |U_{\ell_\alpha N_i}|^2 M_{N_i}$.

- The **sterile neutrino** subclass inherits from the neutrino (HNL) class and represents the main particle of interest in this study and hence is by far the most detailed. The sterile neutrino subclass initialises the 'flavour' property (n_1, n_2, n_3). The sterile neutrino mass is also initialised here. The plentiful decay widths of the sterile neutrino are defined as follows.
  - **General helper functions:**
    - **lam(a,b,c)**: Kallen function used in the charged current integral.
    - **_integral_cc(x_u,x_d,x_l)**: performs the integral for the 3-body charged-current decays (equation 23) for use in the decay width calculation.
    - **_get_nc_coeffs(f,is_int,m)**: returns the neutral-current coefficients C_1, C_2 from table 3, for use in the decay width function.
    - **_L_function(x)** : function used in the neutral current decay width (equation 26).
  - **calculate_decay_width(outgoings, model)**:
    - Categorises the user provided final particle states (single channel calculation), by counting the number of provided particles: charged leptons, neutrinos, quarks, mesons and ALPs.
    - Uses a match/case switch on the above outgoing particle signature to apply the correct decay formula (CC/NC, leptonic, hadronic and the ALP channels). Each branch retrieves the active-sterile mixing angle U_α and CKM matrix element V_{ij} from the Model.py module and applies them in the decay formulas as required.
  - **Channel Lists:** generates lists of all possible final-state 'Particle' instances for each of the below categories, used by the grouped and later total decay-width calculation methods.
    - **_get_invisible_channels** :$(\nu_\alpha \nu_\beta \nu_\beta) channels$

    - **_get_charged_leptonic_channels**
    - **_get_exclusive_hadronic_channels** (generates the single meson hadronic decays for $m_N < 2\text{GeV}$).
    - **_get_inclusive_quark_channels** (generates the channels for hadronic decays $m_N > 2\text{GeV}$ using the decay into quarks + Δ_{QCD} correction method.)
- **Grouped Width Methods:** Use the above lists of channels to obtain grouped decay-widths for each decay category are calculated (applying kinematic choices exclusive/inclusive and QCD corrections).
    - **get_invisible_width** (3ν final state, equation 27)
    - **get_charged_leptonic_width** (three body charged current and neutral current decays, equations 23 and 26)
    - **get_hadronic_width** : Both exclusive single meson and inclusive quark hadronic decay widths(equations 23 and 28-31).
    - **get_ALP_width** : ALP decay (equation 45)
    - **get_total_decay_width** : Sums over all of the above decay widths.
- **get_branching_ratio**: Computes $\frac{\text{Partial Decay Width}}{\text{Total Decay Width}}$

This Particles file thus forms the computational core of the HNL+ALP phenomenology, cleanly implementing particle definitions, kinematics and mixing matrices.

5.2 Model Parameters Python File

The ModelParameters class acts as a central repository for all the fundamental constants (in terms of GeV as is standard in Particle Physics) and user-configurable inputs which define the physical scenario. Upon activation, it initialises

- **Physical Constants**:
    - **Planck Mass**: $M_{\text{pl}} = 2.435 * 10^{18}$ GeV.
    - **Fermi Constant**: $G_F = 1.166 * 10^{-5}$ GeV^{-2}.
    - **Weinberg Angle**: $\sin^2(\theta_W) = 0.2312$.
- **HNL Parameters**:
    - Sets the HNL mass (GeV) to be used in the simulations.
- **ALP Parameters**:
    - Sets the ALP mass m_a.
    - Sets the ALP decay constant f_a.
- **Matrices**
    - **Cabibbo–Kobayashi–Maskawa matrix** : The 3x3 quark mixing matrix, indiced as V_{ij} in the code, is used when calculating HNL decays into Mesons.
    - **Active-sterile mixing Matrix**: A 3x3 active-sterile mixing matrix of $|U_{\ell N}|^2$ values which controls how each sterile flavour (N_1, N_2, N_3) mixes with the active flavours (e, μ, τ). These crucial values enter every partial width formula.

By combining all of these parameters inside the ModelParameters class, the remainder of the engine can be written generically in terms of **params.x**, and any systematic variation, such as scanning over a range of HNL masses, can be implemented simply by assigning different values to the ModelParameters class on the fly, before constituting the model.

5.3 Relativistic Degrees of Freedom CSV file

Simply contains a csv file containing the relativistic degrees of freedom $g_*(T)$ and the corresponding temperature data from Table 8.

5.4 Relativistic Degrees of Freedom Python file

- Uses the Pandas package to extract the $g_*(T)$ and temperature (T) data from the above defined csv file.
- Parameterises the temperature in terms of $z = m_N/T$.
- Uses SciPy interpolate to create a smooth $g_*(T)$ function.

5.5 Model Python File

This file contains the Model class which takes the above model parameters class as an input and uses it to generate the general physical and cosmological functions that will be inputted into the particles module, to generate decay widths. The model class will also be inputted into the plotting file to showcase the various particle physics and cosmology scenarios. The model classes key responsibilities are to

- **Initialisation**
  - Stores the passed ModelParameters object.
  - Constructs an instance of the Relativistic Degrees of Freedom (DOF) class, which reads a CSV file containing $g_*(T)$ and temperature columns. These values are then interpolated into a smooth effective relativistic DOF function, expressed in terms of $z = \frac{m_N}{T}$.
- **Particle Factories**
  - Initialises instances of the particle species with masses and decay constants drawn from 'params'. This implementation was chosen to ensure consistency, so that a particle with dynamically set properties is universally returned for use across the engine.
- **QCD Corrections**
  - **alpha_s(m_N)** implements the one-loop running strong coupling $\alpha_s(m_N)$ with flavour thresholds at charm and bottom quark mass thresholds (equation 40).
  - **get_qcd_correction(m_N)** builds on alpha_s(Q) to compute the higher-order factors used when approximating inclusive hadronic decays for $m_N > 2$ GeV (equation 33).

- **Cosmological Functions**
  - **entropy_density(z)** (equations 61 and 66) computes the background entropy as functions of $z = \frac{m_N}{T}$ using $g_*(T)$ from the RelDegreesOfFreedom calculator.
- **Mixing**
  - **get_U_alpha(sterile, lepton)** looks up the appropriate entry in params.U_matrix to get the active-sterile mixing angle for a given decay channel.
- **Kinematics**
  - **check_kinematics(incoming, outgoing_list)** enforces that the sum of the outgoing particle masses is less than the incoming particle mass, and raises an error if this is requirement is violated. This function is placed as the first step of every simulation to ensure that computation time is not wasted.
- **Light Neutrino Masses**
  - **create_light_neutrino(sterile_flavor, light_flavor)** builds a LightNeutrino instance whose mass is determined by the seesaw relation $|U|^2 m_N$, this mixing parameter dependent mass is what requires the LightNeutrino instance to be initialised inside the Model class. The light neutrino particle class in the Particles module then calls this model result to set its light neutrino masses.

Combined, these methods allow the rest of the engine to remain agnostic of how mass, couplings and the relativistic degrees of freedom are provided. All that is required is to

- Construct a Model(params, csv_path).
- Call its methods to calculate decay widths, cosmological rates or particle instances consistent with the user's chosen benchmarks.

5.6 Plotting File

The Plotting class encapsulates all the high-level plotting routines for HNL+ALP phenomenology. Each method instantiates a new model instance at the chosen HNL mass and allows for the dynamic rescaling of chosen model parameters. Finally, the class generates detailed matplotlib figures. The key features of this class are as follows.

__init__(self, model_params: ModelParameters, g_starcsv_path: str)

- Initalises the class.
- Binds the ModelParameters and path to the relatistic degrees of freedom CSV.
- Construct a local factory map from particle classes to the corresponding Model.create_ methods, so that an arbitrary particle class can be instantiated uniformly throughout the simulation.

Plotting the QCD correction

- For each mass, calls Model.get_qcd_correction(mass), to obtain alpha_s(mass).

– Masks out NaN values for invalid parameters, then plots on log-log axes and saves the figure as "qcd_correction.png".

Plotting Relativistic degrees of freedom

– plot_g_star(self, model: Model, z_range: np.ndarray).

– Calls model.get_g_star(z_range) to obtain the interpolated relativistic degree of freedom (g_* function).

– Plots g_* vs z on a log-linear x-axis.

Plot Thermally Averaged Decay Rates

– The plotter function is defined as plot_thermally_averaged_decay_rates(self, m_N: float, z_range: np.ndarray).

– The function plots $\gamma(z)$, for both the SM and ALP channels, summing over all three sterile flavours.

HNL Iso-lifetime Curve
The function plot_lifetime_iso_lines() generates iso-lifetime contours for the HNL in the mass and active sterile mixing parameter plane $(m_N, |U_{\ell N}|^2)$, for the HNL lifetimes at chosen values (e.g. 0.1,1,10 seconds). The algorithm is implemented as follows

– Generate n_masses values of m_N, between mN_min and mN_max.

– For each, set $|U_{\ell N}|^2 = 1$ for the chosen sterile neutrino initially and then rebuild the model and compute Γ_{tot}.

– For each user-specified HNL lifetime τ solve

$$|U_{\ell N}|^2 = \frac{\hbar}{\tau \Gamma_{\text{tot}}(m_N, |U_{\ell N}|^2 = 1)}. \tag{72}$$

Combined SM and ALP Branching Ratios:
plot_combined_branching() sums over all decay-widths for the three sterile neutrino flavours (N_1, N_2, N_3) for the SM and ALP channels and plot both on log-log axes.

$$BR_{N \to SM} = \frac{\Gamma_{N \to SM}}{\Gamma_{total}}. \tag{73}$$

Fermi Theory Error:
Generates Figure 2, the relative error in the matrix element squared of the fermi approximation in comparison to the full weak propagator, expressed as a function of HNL mass m_N.

5.7 Simulation.py

This file provides the execution layer for the HNL-ALP phenomenology engine. It combines the physics engine (Model, Particles) and the visualisation layer (Plotting). It provides a series of tasks that the user can run. Once the user sets **"TASK TO**

RUN" to the task of interest, the simulation is triggered from the command line using: **python -m OOP.Simulation**. Some of the key simulation properties are

- All tasks construct a fresh Model instance each time they change a parameter. This ensures that a changed parameter in one tasks does not affect the others.
- Kinematic or type errors are reported and return 0.0, so that a failing channel does not crash the full scan. This is useful as at certain kinematic thresholds, some channels are not valid.

Below is a detailed description of the design and implementation of this Simulation class.

- **Imports**
  - numpy, path
  - Classes : Model, Modelparameters, Plotting- which implement the physics.
- **Design**
  - The simulation layer never changes the global state inside the physics classes. Instead it copies the base parameters object and changes an individual setting such as mass, mixing, when needed for a run. This keeps the runs reproducible and as modular as possible.
- **Initialisation**:
  - Stores a reference instance of the provided Model.
- **calculate_partial_width()**
  - Computes the partial decay width for a specified decay channel.
  - **Inputs**: parameters already set by the Model And Particles classes.
    - **incoming_particle**: SterileNeutrino('n1') / ALP
    - **outgoing_particles**: a user provided list such as [Electron, LightNeutrino, LightNeutrino].
  - **Algorithm**
    - Calls _particle.calculate_decay_width(outgoing_particles, self.model).
    - Any kinematic or type errors are caught and reported with a descriptive message.
    - If an error is caught, the method returns 0.0 for the channels partial decay-width.
  - **Output**
    - Returns the partial decay-width (GeV) and prints a formatted line with the channel and numerical value.

calculate_total_width()

- **Purpose**
  - Computes the total width Γ_{tot} by delegating to the Particles class grouped-channel summation.

- **Algorithm**
  - Calls incoming_particle.get_total_decay_width(self.model.
  - If positive it converts the decay-width to a lifetime.
  - Prints both the Γ_{tot} and lifetime τ values and returns Γ_{tot}.
  - Exceptions are caught and reported, 0.0 is returned in case of failure.

run_full_channel_analysis()

- Reuses the above two methods to print:Γ_{partial}, Γ_{total}
- Uses the above to calculate the branching ratio

$$\text{BR} = \frac{\Gamma_{\text{partial}}}{\Gamma_{\text{total}}} \tag{74}$$

Main execution segment (if __name__ == "__main__":) This code block sets up the file paths, constructs the model parameters and dispatches it into a chosen analysis (task). It takes the following classes as inputs

- **Model Parameters**
  - base_params = ModelParameters() provides the physical constants, mixing, default masses,etc. The script optionally changes individual values, depending on the scenario.
- **Relativistic g(T)**
  - Uses Path(__file__).parent and a fallback to find the rel_degree_of_Freedom.csv file. The resolved path is passed into the Model and Plotting classes to define the cosmological quantities.
- **Task selection via 'match TASK_TO_RUN**
  A single string literal controls which analysis is executed by the engine. This ensures that reproducing results for various initial conditions is as trivial as possible. The available tasks are listed in the code as follows
- **"SINGLE_CALCULATION":** Calculates the partial decay-width, full decay-width and branching ratio for a user-specified channel,
  by running the Simulation.run_full_channel_analysis(...) described above.
- **"PLOT_BRANCHING_RATIOS_HADRONS":** plots the branching ratio for exclusive hadronic decays, for a range of HNL masses up to 1 GeV,
  using Plotting.plot_branching_ratios(...)
- **"PLOT_BRANCHING_RATIOS_QUARKS"**: plots the inclusive (quark-level), 3ν and ALP branching ratios using Plotting.plot_quark_level_branching_ratios(...).
- **"PLOT_QCD_CORRECTION_VS_MASS"**: Calls Plotting.plot_qcd_correction(...) to output the Δ_{QCD} correction factor as a function of m_N.

- **"PLOT_REL_DEGREES_OF_FREEDOM_VS_Z"**: Builds an instance of the Model and calls Plotting.plot_g_star(model, z_range) to show $g_*(z)$ across relevant cosmological range.
- **"PLOT_THERMALLY_AVERAGED_WIDTHS"**: plots the thermally averaged decay rates using Plotting.plot_thermally_averaged_decay_rates(m_N, z_range) which sums over all sterile flavours and includes thermal averaging and equilibrium densities.
- **"LIFETIME_CONTOUR_PLOT"**: Calls Plotting.plot_lifetime_iso_lines(...) to plot iso-lifetime contours for the HNLs in the $(m_N, |U_{\ell N}|^2)$ plane.
- **"PLOT_COMBINED_BRANCHING_RATIO_SM_ALP"**: Plots the branching ratios for the full SM and ALP decays of the HNLs using Plotting.plot_combined_branching(mass_range).
- **"Plot_Fermi_Theory_Error"**: plots the relative error between the fermi contact theory approximation and the full propagator (equation 22) as shown in Figure 2.
- **Incorrect Input**: If a task is incorrectly chosen, the following message is printed "Error: Unknown task 'TASK_TO_RUN'. Please choose a valid task."

5.8 Benchmarks

Before we add the exotic ALP decays, let us first consider the base case of the three HNL flavours decaying only into SM particles. To ensure the accuracy of the model the HNL branching ratios into light neutrinos (invisible channel), leptons, π, η, ρ, K channels were simulated in Figure 10 and 11 below and they matched the results in the literature [20]. As expected we see in Figure 10 that the decays into light neutrinos $N \to \nu\bar{\nu}\nu$ dominates at low HNL masses with a smaller contribution from the available leptonic channel $N \to \nu_e e\bar{\nu}_e$. Once the HNL mass rises above the pion mass $\pi^{\pm} = 139.6$MeV. The pion channel quickly becomes dominant. As expected the η, ρ, K channels activate once their mass-thresholds are met. In Figure 11 we see that at HNL masses above 1 GeV, the hadronic decays dominated over the leptonic and light-neutrino channels.

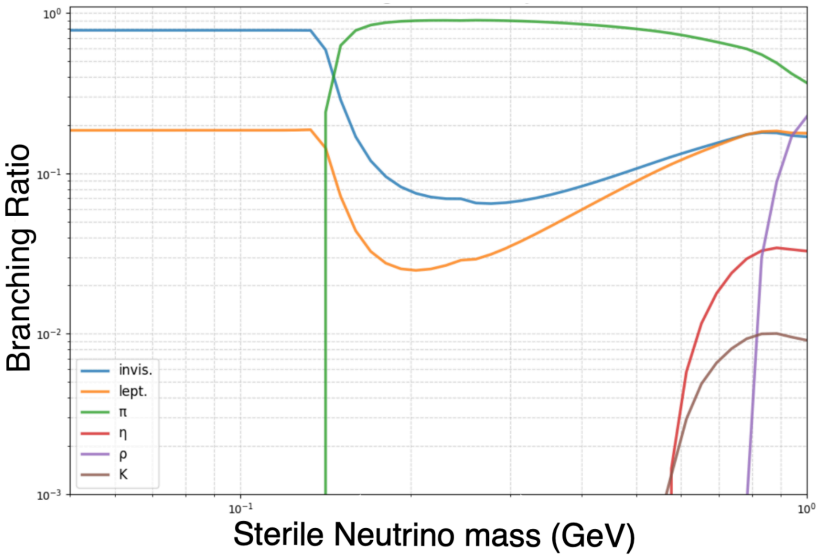

Figure 10: HNL branching ratios into SM particles only as a function of heavy neutrino mass m_N.

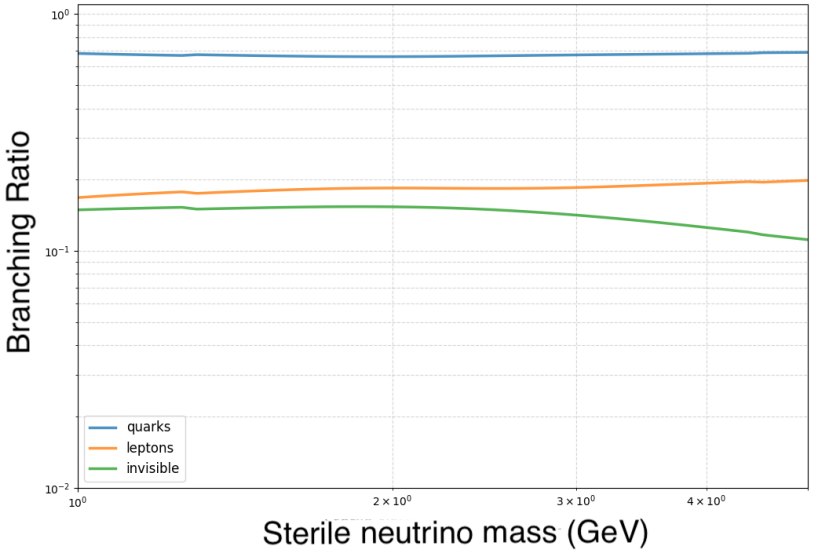

Figure 11: HNL branching ratios into SM particles only as a function of heavy neutrino mass m_N.

6 Results

6.1 HNL Lifetimes

The primary motivation behind introducing the ALP decay channel is to allow the HNLs to decay before they can affect BBN abundances. In Figure 12 we can see the contour iso-lifetime plots for the HNLs, which display the mass and active-sterile mixing angles required for a particular HNL lifetime. We can see that there are significant differences in magnitude between the contours of the N_1, N_2, N_3 iso-lifetime curves. The N_3 contour correctly only begins for M_N values of atleast m_τ. By comparing our $(m_{N_2}, |U_{\ell N_2}|^2)$ contour (Figure 12) containing the dominant ALP decay to the literature of past experiments and BBN, Seesaw bounds (figure 1), we can see that there maybe a slight portion of the parameter space accessible for our N_2 HNL at low masses (~ 0.1 GeV), for the case where the N_2 HNLs mix exclusively with the μ lepton flavour.

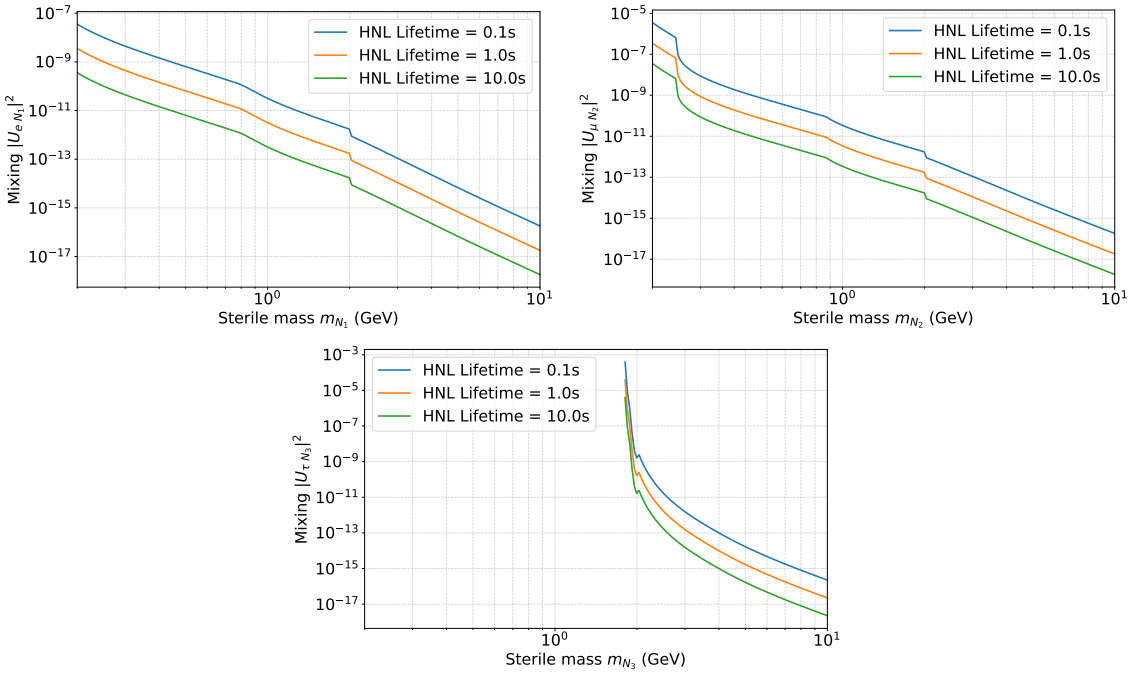

Figure 12: (Top left) N_1, HNL (top right) N_2, HNL (bottom) N_3 HNL. Iso-lifetime contour plot in the $(m_N, |U_{\ell N}|^2)$.

6.2 Total Branching Ratios

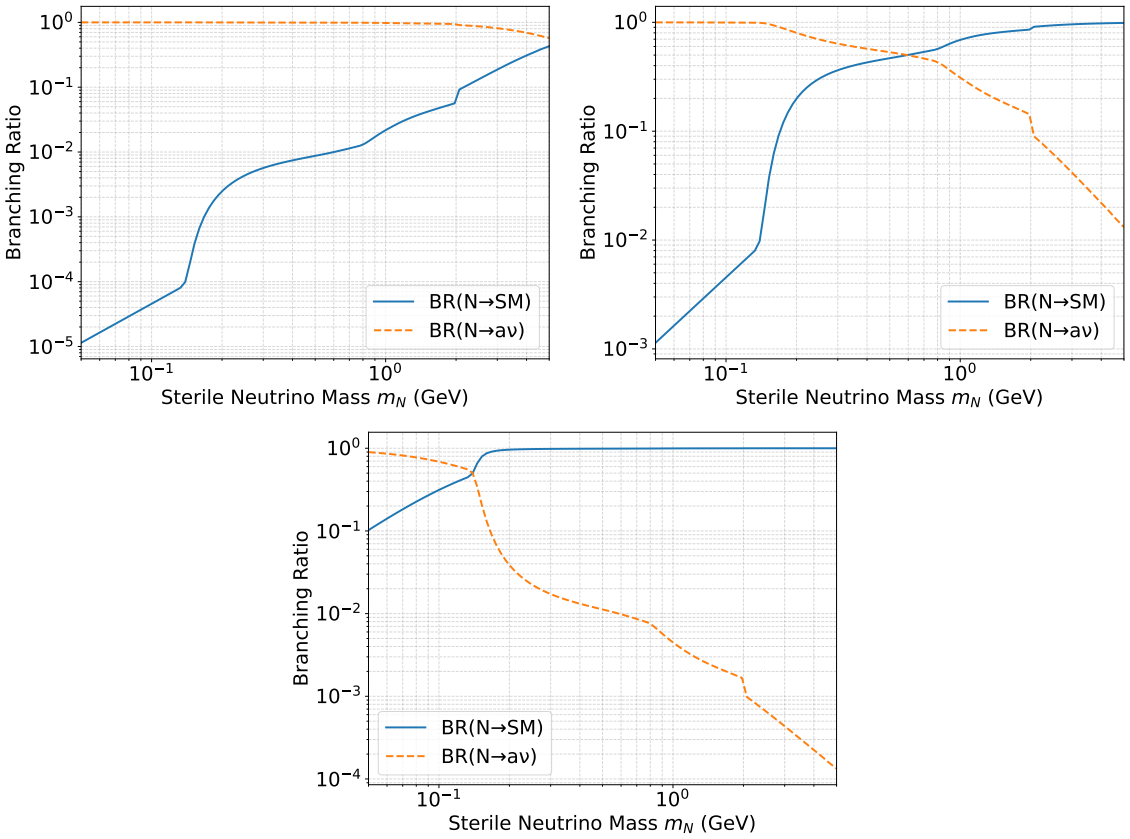

Figure 13: Combined Branching ratios for mixing angle $|U_{\ell N}|^2 = 10^{-10}$, at decay constants $f_a = 10^5$GeV subplot (a), $f_a = 10^6$GeV subplot (b) , $f_a = 10^7$GeV subplot (c).

In Figure 13 above we can see the total branching ratios into SM and ALP channels for the combined HNL flavours (n_1, n_2, n_3). We can see that the branching ratios into SM channels, and ALPs are approximately equal for $f_a = 10^6$GeV at around $m_N = 0.6$GeV. With the ALP decays dominating for lower m_N values and SM decays dominating for higher m_N values. For $f_a = 10^5$ GeV we can see that the ALP decays dominate up to $m_N = 5$ GeV. For $f_a = 10^7$ GeV we can see that above $m_N = 0.2$ GeV, the decays into SM particles dominate.

6.3 Thermally averaged decay rates

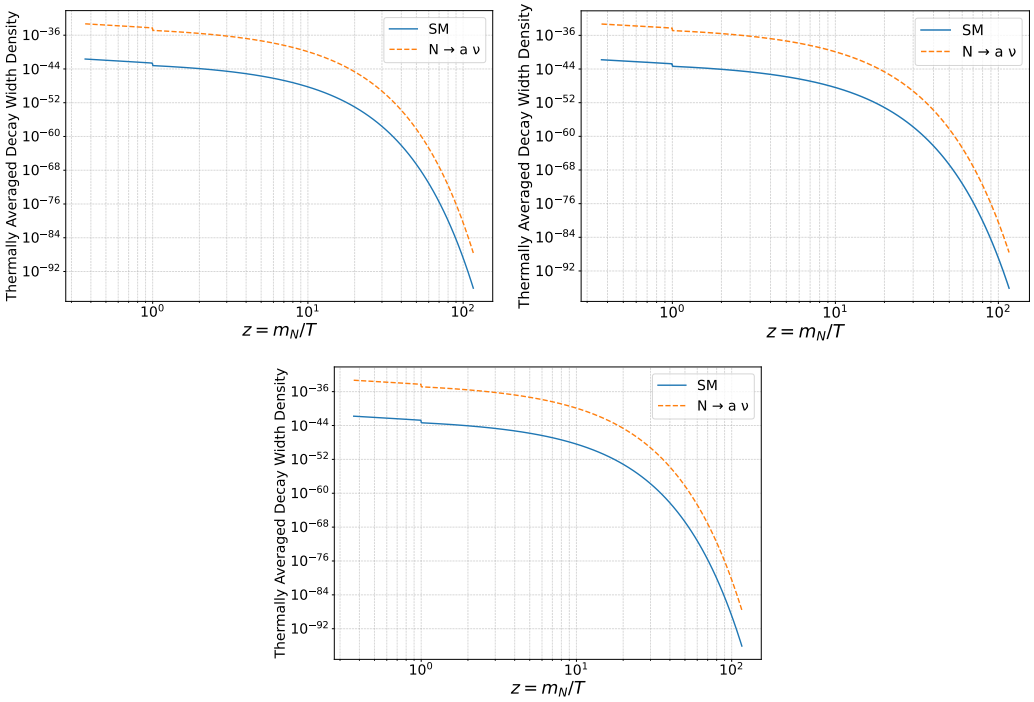

Figure 14: Thermally averaged decay widths into the combined SM + ALP channels for individual heavy neutrino flavours (N_1, N_2, N_3) ,mixing with only one active generation each (e, ν, τ). (Top left) N_1 HNL, (top right) N_2 HNL, (bottom) N_3 HNL. The parameters for each HNL flavour were set to $m_N = 0.5$ GeV and $|U_{\ell N}|^2 = 10^{-10}$.

The plots appear near identical, with only slight numerical differences within one order of magnitude. This is expected due lepton universality. We can see that at late times the rates fall to negligible levels, which is as expected, given the difficulty in trying to observe these exotic particles in the current day.

7 Conclusions and Outlook

In this research thesis a Python engine was developed to examine the HNL decay into SM particles and exotic ALPs, building on the work of [19, 20]. The object oriented approach to the programming ensures the possibility of building on this codebase in the future. Through its particle inheritance system and general csv file acceptance for physical inputs such as the relativistic degrees of freedom values. The branching ratios of SM and exotic channels was examined for a variety of HNL and ALP parameters. We found that for active-sterile mixing $|U_{\ell N}|^2 = 10^{-10}$, for an ALP decay constant $f_a = 10^5$ GeV the dominant decay is into ALPs, for HNLs of $m_N < 5$ GeV. For $f_a = 10^6$ GeV the branching ratios into SM and ALPs are equal at $m_N \approx 0.7$ GeV. With ALP decay dominant for lower HNL masses and SM decays dominant for higher HNL masses. For $f_a = 10^7$ GeV the SM decays become dominant at $m_N \sim 0.2$ GeV . HNL Iso-lifetime contours were calculated in the $(m_N, |U_{\ell N}|^2)$ plane, thus showcasing potential promising mass and active-sterile mixing parameters for experimental search, that could avoid the bounds on HNLs set by BBN abundances. BBN limits require HNLs to wash out at $t \lesssim 1$s so that the HNL decays do not inject additional energy to the thermal bath, which would damage neutron abundances. By comparing our $(m_{N_2}, |U_{\ell N_2}|^2)$ contour (figure 12) containing the dominant ALP decay to the literature of past experiments and BBN, Seesaw bounds (figure 1), we can see that their maybe a slight portion of the parameter space accessible for our N_2 HNL at low masses (~ 0.1 GeV), for the case where the N_2 HNL mixes exclusively with the μ lepton flavour. Cosmological analysis features were incorporated in the relativistic degrees of freedom data interpolator and the Model definitions. This was used to calculate the thermally averaged decay rates of the HNL and ALPs, providing a foundation for the works continuation into BBN analysis. As expected by lepton universality the decay rates for each of the HNL flavours were similar to within one order of magnitude. As expected given the difficulty in trying to find these exotic species, their thermally averaged decay rates dropped to negligible levels at late times. A limitation of this study is that it does not consider the decay of SM particles into HNLs, this could be implemented following the work of [20] and would be valuable in an expanded cosmological discussion. Additionally the hard switch from the single meson decays to decays to quarks with a Δ_{QCD} correction at 2 GeV is a rather crude solution. Implementing a smooth transition between the regimes over the range of heavy neutrino masses where the quark + Δ_{QCD} channels go from being appreciable to dominant over the single meson decays would be a more accurate implementation and would be worth adding in an expanded study. An interesting continuation of this work would be to further develop the discussion in ref. [19], by implementing coupled equations for each of the HNL flavours and the ALP, to determine the change in energy densities ρ and number densities n of the particle species, due to the expansion of the universe and particle interactions [41]. An outlook of this idea is provided as follows. The general boltzmann equation form is

$$\frac{dn_i}{dt} + 3Hn_i = C_i[\{n_j\}], \tag{75}$$

where $C_i[\{n_j\}]$ corresponds to the collision terms due to particle interactions which create or destroy the species, like decays and annihilations. Interactions between more than two particles are exceedingly rare and hence, it is reasonably accurate to only consider single-particle decays and two-particle annihilations. The collision factor for species 1 in a reversible,

two-particle annihilation process $1+2 \leftrightarrow 3+4$ is

$$C_1[\{n_j\}] = -\alpha n_1 n_2 + \beta n_3 n_4, \tag{76}$$

where $-\alpha n_1 n_2$ is the annihilation term for particles 1,2 and $\beta n_3 n_4$ is the creation term for particles 1,2 through the reverse process, $\alpha = \langle \sigma v \rangle$ is the thermally averaged cross-section. As $n_i a^3$ remains constant while in chemical equilibrium, the rate of particle creation and annihilation is equal for the reversible process and β can be written as $\beta = \left(\frac{n_1 n_2}{n_3 n_4}\right)_{eq} \alpha$. Therefore, the collision factor can be modified to

$$C_1[\{n_j\}] = -\langle \sigma v \rangle \left[n_1 n_2 - \left(\frac{n_1 n_2}{n_3 n_4}\right)_{eq} n_3 n_4 \right]. \tag{77}$$

In the case of a single-particle decay $1 \to 3+4$, the collision term reduces to

$$C_1[\{n_j\}] = -\Gamma^{1\to 3+4} \left[n_1 - \left(\frac{n_1}{n_3 n_4}\right)_{eq} n_3 n_4 \right]. \tag{78}$$

A set of coupled Boltzmann equations has to be solved numerically for all the particles involved to determine the time evolution of HNL and ALP abundances. Using these densities, the model's impact on BBN could be determined and the HNL mixing parameter $|U_{\ell N}|^2$ and masses may be constrained, which would illustrate the impact of introducing a dominant ALP decay channel on the sensitivity of upcoming HNL experimental searches [6,45]. Writing the boltzmann in terms of the comoving yield, for the three sterile neutrino flavours we get the 4 coupled Boltzmann equations

$$\begin{aligned} \sum_{i=1,2,3} zHs\frac{dY_{N_i}}{dz} = \sum_{i=1,2,3} \Bigg[& -\gamma^{eq}_{N_i N_i \to SM} \left(\frac{Y^2_{N_i}}{Y^{eq,2}_{N_i}} - 1 \right) + \gamma^{eq}_{aa \to N_i N_i} \left(\frac{Y^2_a}{Y^{eq,2}_a} - \frac{Y^2_{N_i}}{Y^{eq,2}_N} \right) \\ & -\gamma_{N_i \to SM} \left(\frac{Y_{N_i}}{Y^{eq}_{N_i}} - 1 \right) - \sum_{\alpha=e,\mu,\tau} \gamma_{N_I \to a\nu_\alpha} \left(\frac{Y_{N_i}}{Y^{eq}_{N_i}} - \frac{Y_a}{Y^{eq}_a} \right), \end{aligned} \tag{79}$$

$$\begin{aligned} zHs\frac{dY_a}{dz} = \sum_{i=1,2,3} \Bigg[& - \sum_{\alpha=e,\mu,\tau} \gamma^{eq}_{aa \to \nu_\alpha \nu_\alpha} \left(\frac{Y^2_a}{Y^{eq,2}_a} - 1 \right) - \gamma^{eq}_{aa \to N_i N_i} \left(\frac{Y^2_a}{Y^{eq,2}_a} - \frac{Y^2_{N_i}}{Y^{eq,2}_{N_i}} \right) \\ & - \sum_{\alpha=e,\mu,\tau} \gamma_{a \to \nu\nu} \left(\frac{Y_a}{Y^{eq}_a} - 1 \right) + \sum_{\alpha=e,\mu,\tau} \gamma_{N_i \to a\nu} \left(\frac{Y_{N_i}}{Y^{eq}_{N_i}} - \frac{Y_a}{Y^{eq}_a} \right). \end{aligned} \tag{80}$$

Where Y is the co-moving yield, s is the entropy, H is the Hubble parameter and γ is the thermally averaged rate.

References

[1] S. Davidson, E. Nardi, and Y. Nir, "Leptogenesis," *Physics Reports*, vol. 466, no. 4-5, pp. 105–177, 2008.

[2] M. Fukugita and T. Yanagida, "Barygenesis without grand unification," *Physics Letters B*, vol. 174, no. 1, pp. 45–47, 1986.

[3] S. Pascoli, S. T. Petcov, and A. Riotto, "Leptogenesis and low energy cp-violation in neutrino physics," *Nuclear physics B*, vol. 774, no. 1-3, pp. 1–52, 2007.

[4] C. Adams, D. Adams, T. Akiri, T. Alion, K. Anderson, C. Andreopoulos, M. Andrews, I. Anghel, J. C. C. d. Anjos, M. Antonello *et al.*, "The long-baseline neutrino experiment: exploring fundamental symmetries of the universe," *arXiv preprint arXiv:1307.7335*, 2013.

[5] P. Mermod, "Hidden sector searches with ship and na62," *arXiv preprint arXiv:1712.01768*, 2017.

[6] E. C. Gil, Kleimenova *et al.*, "Search for k+ decays to a muon and invisible particles," *Physics Letters B*, vol. 816, p. 136259, 2021.

[7] M. Drewes, J. Hajer, J. Klaric, and G. Lanfranchi, "Na62 sensitivity to heavy neutral leptons in the low scale seesaw model," *Journal of High Energy Physics*, vol. 2018, no. 7, 2018.

[8] S. Alekhin, W. Altmannshofer, T. Asaka, B. Batell, F. Bezrukov, K. Bondarenko, A. Boyarsky, K.-Y. Choi, C. Corral, N. Craig *et al.*, "A facility to search for hidden particles at the cern sps: the ship physics case," *Reports on Progress in Physics*, vol. 79, no. 12, p. 124201, 2016.

[9] M. Anelli, S. Aoki, G. Arduini, J. Back, A. Bagulya, W. Baldini, A. Baranov, G. Barker, S. Barsuk, M. Battistin *et al.*, "A facility to search for hidden particles (ship) at the cern sps," *arXiv preprint arXiv:1504.04956*, 2015.

[10] V. V. Gligorov, S. Knapen, M. Papucci, and D. J. Robinson, "Searching for long-lived particles: a compact detector for exotics at lhcb," *Physical Review D*, vol. 97, no. 1, p. 015023, 2018.

[11] J. P. Chou, D. Curtin, and H. Lubatti, "New detectors to explore the lifetime frontier," *Physics Letters B*, vol. 767, pp. 29–36, 2017.

[12] D. Curtin and M. E. Peskin, "Analysis of long-lived particle decays with the mathusla detector," *Physical Review D*, vol. 97, no. 1, p. 015006, 2018.

[13] J. A. Evans, "Detecting hidden particles with mathusla," *Physical Review D*, vol. 97, no. 5, p. 055046, 2018.

[14] J. C. Helo, M. Hirsch, and Z. S. Wang, "Heavy neutral fermions at the high-luminosity lhc," *Journal of High Energy Physics*, vol. 2018, no. 7, pp. 1–23, 2018.

[15] J. L. Feng, I. Galon, F. Kling, and S. Trojanowski, "Forward search experiment at the lhc," *Physical Review D*, vol. 97, no. 3, p. 035001, 2018.

[16] Feng, "Dark higgs bosons at faser," *arXiv preprint arXiv:1710.09387*, 2017.

[17] F. Kling and S. Trojanowski, "Heavy neutral leptons at faser," *Physical Review D*, vol. 97, no. 9, p. 095016, 2018.

[18] A. et al, "Planck2018 results: Vi. cosmological parameters," *Astronomy & Astrophysics*, vol. 641, p. A6, Sep 2020.

[19] F. F. Deppisch and Gonzalo, "Relaxing limits from big bang nucleosynthesis on heavy neutral leptons with axion-like particles," *Journal of Cosmology and Astroparticle Physics*, vol. 2025, no. 02, p. 054, 2025.

[20] K. Bondarenko and Boyarsky, "Phenomenology of gev-scale heavy neutral leptons," *Journal of High Energy Physics*, vol. 2018, no. 11, 2018.

[21] M. Thomson, *Modern particle physics*. Cambridge University Press, 2013.

[22] "Test of lepton universality in beauty-quark decays," *Nature Physics*, vol. 18, no. 3, pp. 277–282, 2022.

[23] J. Schechter and J. W. Valle, "Neutrino masses in su (2) u (1) theories," *Physical Review D*, vol. 22, no. 9, p. 2227, 1980.

[24] N. Sabti and Magalich, "An extended analysis of heavy neutral leptons during big bang nucleosynthesis," *Journal of Cosmology and Astroparticle Physics*, vol. 2020, no. 11, p. 056, 2020.

[25] A. M. Sirunyan, A. Tumasyan, W. Adam, F. Ambrogi, E. Asilar, T. Bergauer, J. Brandstetter, E. Brondolin, M. Dragicevic, J. Erö *et al.*, "Search for heavy neutral leptons in events with three charged leptons in proton-proton collisions at s= 13 tev," *Physical review letters*, vol. 120, no. 22, p. 221801, 2018.

[26] A. Blondel, E. Graverini, N. Serra, and M. Shaposhnikov, "Search for heavy right handed neutrinos at the fcc-ee," *Nuclear and particle physics proceedings*, vol. 273, pp. 1883–1890, 2016.

[27] C. Ahdida, R. Albanese, A. Alexandrov, A. Anokhina, S. Aoki, G. Arduini, E. Atkin, N. Azorskiy, F. Baaltasar Dos Santos, J. Back *et al.*, "Sensitivity of the ship experiment to heavy neutral leptons," *Journal of High Energy Physics*, vol. 2019, no. 4, pp. 1–20, 2019.

[28] D. Curtin, M. Drewes, M. McCullough, P. Meade, R. N. Mohapatra, J. Shelton, B. Shuve, E. Accomando, C. Alpigiani, S. Antusch *et al.*, "Long-lived particles at the energy frontier: the mathusla physics case," *Reports on progress in physics*, vol. 82, no. 11, p. 116201, 2019.

[29] A. Dolgov, S. Hansen, G. Raffelt, and D. Semikoz, "Heavy sterile neutrinos: bounds from big-bang nucleosynthesis and sn 1987a," *Nuclear Physics B*, vol. 590, no. 3, pp. 562–574, 2000.

[30] V. Gribanov, S. Kovalenko, and I. Schmidt, "Sterile neutrinos in tau lepton decays," *Nuclear Physics B*, vol. 607, no. 1-2, pp. 355–368, 2001.

[31] A. Atre, T. Han, S. Pascoli, and B. Zhang, "The search for heavy majorana neutrinos," *Journal of High Energy Physics*, vol. 2009, no. 05, p. 030, 2009.

[32] J. C. Helo, S. Kovalenko, and I. Schmidt, "Sterile neutrinos in lepton number and lepton flavor violating decays," *Nuclear Physics B*, vol. 853, no. 1, pp. 80–104, 2011.

[33] R. E. Shrock, "General theory of weak processes involving neutrinos. ii. pure leptonic decays," *Physical Review D*, vol. 24, no. 5, p. 1275, 1981.

[34] G. Källén, "Elementary particle physics," *(No Title)*, 1964.

[35] R. Workman, V. Burkert, V. Crede, E. Klempt, U. Thoma, L. Tiator, K. Agashe, G. Aielli, B. Allanach, C. Amsler, M. Antonelli, E.-C. Aschenauer, D. Asner, H. Baer, S. Banerjee, R. Barnett, L. Baudis, C. Bauer, and P. Zyla, "Review of particle physics," *Progress of Theoretical and Experimental Physics*, vol. 2022, 08 2022.

[36] B. Colquhoun, C. Davies, J. Kettle, J. Koponen, A. Lytle, R. Dowdall, G. Lepage, and H. Collaboration), "B-meson decay constants: a more complete picture from full lattice qcd," *Physical Review D*, vol. 91, no. 11, p. 114509, 2015.

[37] R. Workman, P. D. Group *et al.*, "Prog. theor," *Exp. Phys*, vol. 2022, no. 8, p. 083C01, 2022.

[38] S. Navas, C. Amsler, T. Gutsche, C. Hanhart, J. Hernández-Rey, C. Lourenço, A. Masoni, M. Mikhasenko, R. Mitchell, C. Patrignani *et al.*, "Review of particle physics," *Physical Review D*, vol. 110, no. 3, p. 030001, 2024.

[39] Y. Schröder and M. Steinhauser, "Four-loop decoupling relations for the strong coupling," *Journal of High Energy Physics*, vol. 2006, no. 01, p. 051, 2006.

[40] K. Chetyrkin, J. H. Kühn, and C. Sturm, "Qcd decoupling at four loops," *Nuclear Physics B*, vol. 744, no. 1-2, pp. 121–135, 2006.

[41] D. Baumann, *Cosmology*. Cambridge University Press, 2022.

[42] L. Husdal, "On effective degrees of freedom in the early universe," *Galaxies*, vol. 4, no. 4, p. 78, 2016.

[43] E. Hubble, "A relation between distance and radial velocity among extra-galactic nebulae," *Proceedings of the national academy of sciences*, vol. 15, no. 3, pp. 168–173, 1929.

[44] J. Wawrzynek, "MSc Thesis: Source Code," https://github.com/janwawrzynek/UCL_MSc_Thesis, 2025.

[45] A. A. Abud, Abi *et al.*, "Deep underground neutrino experiment (dune) near detector conceptual design report," *Instruments*, vol. 5, no. 4, p. 31, 2021.